NAVAL POSTGRADUATE SCHOOL
Monterey, California

THESIS

ANNEALING OF RADIATION DAMAGED GALLIUM ARSENIDE SOLAR CELLS BY LASER ILLUMINATION

by

Richard Dillon Kramer

September, 1994

Thesis Advisor: Sherif Michael

REPORT DOCUMENTATION PAGE	Form Approved OMB No. 0704

1. AGENCY USE ONLY *(Leave blank)*	2. REPORT DATE September 1994	3. REPORT TYPE AND DATES COVERED Master's Thesis

4. TITLE AND SUBTITLE : ANNEALING OF RADIATION DAMAGED GALLIUM ARSENIDE SOLAR CELLS BY LASER ILLUMINATION (U)	5. FUNDING NUMBERS
6. AUTHOR(S) Kramer, Richard D.	
7. PERFORMING ORGANIZATION NAME(S) AND ADDRESS(ES) Naval Postgraduate School Monterey CA 93943-5000	8. PERFORMING ORGANIZATION REPORT NUMBER
9. SPONSORING/MONITORING AGENCY NAME(S) AND ADDRESS(ES)	10. SPONSORING/MONITORING AGENCY REPORT NUMBER

11. SUPPLEMENTARY NOTES The views expressed in this thesis are those of the author and do not reflect the official policy or position of the Department of Defense or the U.S. Government.

12a. DISTRIBUTION/AVAILABILITY STATEMENT Approved for public release; distribution unlimited	12b. DISTRIBUTION CODE A

13. ABSTRACT *(maximum 200 words)* In this research, preliminary results of a new approach for annealing previously irradiated Gallium Arsenide solar cells is reported. This technique examines the use of laser illumination to induce Forward-Biased current annealing. Five GaAs solar cells were irradiated with 65 MeV electrons at varying fluence levels. Visible laser light produced a 0.5 A/cm^2 forward-biased current density and raised the solar cell temperature by 30°C. Ten to fifteen percent recovery of degraded parameters was achieved in four of the five tested cells. The results show that a laser can produce some annealing in radiation damaged GaAs solar cells. Further investigation into the results also indicate that the 65 MeV energy level of the electron irradiation could have caused unrecoverable permanent damage to the solar cells. Follow up research of this annealing technique should be conducted on GaAs cells that are being irradiated at a lower energy level as well as lower fluence level. Repetitive annealing of lightly damaged cells in previous research has provided appreciative recovery using forward bias current techniques. One can expect similar results using the laser induced annealing technique proposed in this research.

14. SUBJECT TERMS Gallium Arsenide, Solar Cells, Annealing, Lasers	15. NUMBER OF PAGES 91
	16. PRICE CODE

17. SECURITY CLASSIFICATION OF REPORT	18. SECURITY CLASSIFICATION OF THIS PAGE	19. SECURITY CLASSIFICATION OF ABSTRACT	20. LIMITATION OF ABSTRACT
Unclassified	Unclassified	Unclassified	UL

NSN 7540-01-280-5500

Standard Form 298 (Rev. 2-89)
Prescribed by ANSI Std. 239-18

Approved for public release; distribution is unlimited.

Annealing of Radiation Damaged
Gallium Arsenide Solar Cells by Laser Illumination

by

Richard D. Kramer
Lieutenant Commander, United States Navy
B.S., United States Naval Academy, 1981

Submitted in partial fulfillment
of the requirements for the degree of

MASTER OF SCIENCE IN ELECTRICAL ENGINEERING

from the

NAVAL POSTGRADUATE SCHOOL
September 1994

Author: 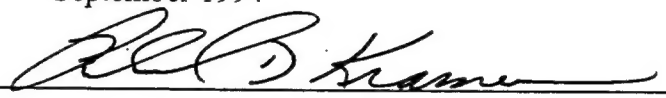

Richard D. Kramer

Approved by: 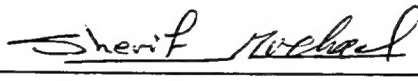

Sherif Michael, Thesis Advisor

Robert Ashton, Second Reader

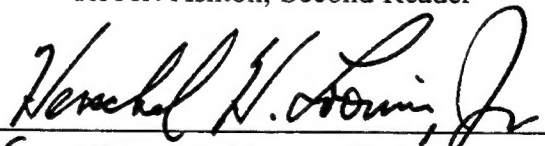

for Michael A. Morgan, Chairman
Department of Electrical and Computer Engineering

ABSTRACT

In this research, preliminary results of a new approach for annealing previously irradiated Gallium Arsenide solar cells is reported. This technique examines the use of laser illumination to induce Forward-Biased current annealing. Five GaAs solar cells were irradiated with 65 MeV electrons at varying fluence levels. Visible laser light produced a 0.5 A/cm^2 forward-biased current density and raised the solar cell temperature by 30°C. Ten to fifteen percent recovery of degraded parameters was achieved in four of the five tested cells. The results show that a laser can produce some annealing in radiation damaged GaAs solar cells. Further investigation into the results also indicate that the 65 MeV energy level of the electron irradiation could have caused unrecoverable permanent damage to the solar cells. Follow up research of this annealing technique should be conducted on GaAs cells that are being irradiated at a lower energy level as well as lower fluence level. Repetitive annealing of lightly damaged cells in previous research has provided appreciative recovery using forward bias current techniques. One can expect similar results using the laser induced annealing technique proposed in this research.

TABLE OF CONTENTS

ACKNOWLEDGMENT

To the memory of my Parents

I. INTRODUCTION

As spacecraft missions continue to advance and their power requirements continue to grow, there is an increasing need for improvements to present day space power system technology. It will not be long before spacecraft will require a 100 kW power source. Though a satellite's typical power generating system provides about 3 kW, space stations will require as much as 300 kW.

The solar cell has been one of the main sources for the generation of electrical power aboard practically all spacecraft. Used for this application, solar cells have their greatest advantage over other power generating sources. Their importance is unquestionable. Solar cells have powered our communications, weather, navigation, surveillance, and military satellites.

The advantages of solar cells include being a reliable, cost-effective, and safe electrical power source as well as having a high power-to-weight ratio compared to other space power systems. Certain disadvantages exist also, such as their low power output per unit area, relatively low cell efficiencies, the need for an alternate power source that is capable of maintaining the system requirements during eclipses, and decreased power performance due to particle radiation found in the space environment.

The degradation of the generated output power of solar cells when exposed to the harsh environment in space shortens the life expectancy of the power system. A considerable amount of research and studies has been devoted to developing new methods to improve cell efficiencies and create a more radiation hardened solar cell that

would increase its lifetime. Research has led to experimenting with different types of semiconductor materials as well as developing new compound materials which reduce the incident energy required by the solar cell to generate the same electrical energy. Manufacturing techniques have evolved which have included the addition of a coverglass on the cell which helps to provide shielding against damaging particle radiation. Solar cell response to illumination, efficiency, and other important parameters are covered in greater detail in Chapter II.

Particle radiation damage to solar cell arrays takes place outside the Earth's atmosphere within the Earth's solar magnetic field where electrons and protons are trapped. These energetic particles cause radiation damage to solar cells resulting in serious degradation of the power performance over the lifetime of a spacecraft. Typical satellite power systems have a lifetime of only six to ten years. The space environment and its effects are discussed in greater detail in Chapter III.

As a consequence of the deterioration of the output power potential of the cell, the designer is required to build significantly larger arrays in order to meet the end-of-life (EOL) power specifications. Larger solar cell array panels translate to more cells and heavier launch payloads, both of which increase the costs appreciably. Generally, what determines the lifetime of a spacecraft is the diminishment or deterioration of its power system: the exhaustion of propellant, battery deterioration, or cell radiation damage. When satellites do reach their end-of-life (EOL), most of the time they are still fully functional and capable of fulfilling their designed mission but, their power system has

deteriorated to a point that they are no longer capable of providing the minimum required power and therefore have to be replaced.

Laboratory research has shown that most, if not all, radiation damage to solar cells could be reversed by annealing the cells at temperatures ranging between 200°C and 400°C depending on the type of cells [Ref. 1:p. 160]. Further research has demonstrated an annealing process, with a more practical space application, that uses a method of periodic current injection [Ref. 2:p. 45] and requires temperatures below 100°C to rejuvenate radiation degraded solar cells. Current injection annealing as well as other accomplished methods of annealing are described in Chapter IV.

To be able to perform on-orbit annealing on spacecraft solar cells would reverse the effects of radiation damage, thus, prolonging the lifetime of spacecraft. The capability to anneal solar cells would eliminate the requirement for over designing the solar arrays in order to meet the minimum power requirement at the EOL. This, of course, would greatly reduce the overall costs by reducing the number of cells required per array, lowering the overall weight at launch, and lessen the need to replace satellites as often as every six years.

There also has been considerable research in the area of using a beam power source on Earth to support and power systems in space. One method that is being considered is to use a ground-based laser directed at solar cell arrays in space. Advances in lasers and optical systems have generated much interest in this field. Many of these proposals and applications are a fall out from Strategic Defense Initiative (SDI), but other research facilities, such as the National Aeronautics and Space Administration (NASA), the

Department of Energy (DOE), and many private companies have continued research and development of lasers with this capability for the purpose of power beaming.

There is great potential in this field. Many of the advantages are listed in References 3 and 4, but of particular importance, as far as solar cell performance is concerned, is the dramatic increase in efficiency of the solar cell under laser illumination. Chapter V goes into greater depth in studying laser light and the performance of solar cells under a monochromatic light source such as a laser.

In order to counteract some of the radiation effects in space and to prolong the lifetime of solar array power systems, a practical annealing technique suitable for on-orbit conditions must be found. Various methods of annealing have been attempted in the past with favorable results, but they have not been suitable or cost-effective to install in a spacecraft. However, these results can be used as a basis for further research in annealing processes.

Earlier research has taught us methods that have produced successful annealing of radiation damaged solar cells. For example, we now know that heat and/or current in a cell will stimulate cell recovery. In 1980, a 75 kilo-watt laser was used to produce annealing in previously irradiated silicon solar cells [Ref. 5:pp. 277-280]. This work used the intense laser light, focused to a 0.17 cm spot size to create enough heat in the solar cell to induce annealing. Of course, even the megawatt lasers in development today would not be able to produce that type of intensity on an orbiting spacecraft.

Previous work has had many common factors involved but none have been practically available for use in space. The goal of this research is to show that lasers can

produce enough self-generated current and will increase the temperature sufficiently to induce annealing where other methods required an external heater.

To simulate the space electron radiation environments a linear accelerator is used. Chapter VI discusses the linear accelerator located at the Naval Postgraduate School and the methods to determine the amount of radiation emitted by the accelerator. Chapter VII discusses the procedures taken to complete this research with the results and conclusions in the final chapters.

II. SOLAR CELLS

A. BANDGAP ENERGY

Solar cells are solid state devices which convert light energy into electric energy through a process called the photovoltaic effect. Solar cells are commonly classified by the type of material from which they are made, silicon and gallium arsenide being the most prevalent.

Every type of solid state material is characterized by its associated bandgap energy level E_g, which is the energy needed to free an electron from the outermost shell of the atom's orbiting electrons thus creating an electron-hole pair in the process. Solar cells receive this energy in the form of light (photons). The energy hv, where h is Planck's constant, of a photon is related to the frequency v of the light wave by equation 2.1.

$$h \times v = h \times (c/\lambda) = 1.24/\lambda(\mu m) \qquad \text{(in electron volts)} \qquad (2.1)$$

where c is the speed of light and λ is the light wavelength. If the interacting photon has an energy greater than the bandgap of the solar cell, $hv > E_g$, and if a collision with a valence electron occurs, the electron will absorb the photon energy. This energy is consumed by raising a valence-band electron into the conduction band and creating an electron-hole pair. The electrons in the conduction band are "free" to move and establish the external current. Figure 2-1 [Ref. 7:p. 17] shows the interactions within a cell. [Ref. 6:pp. 44-45]

A photon having hv greater than E_g is capable of generating only one electron-hole pair. The excess energy is given off as heat. Photons with hv less than E_g are not absorbed by the solar cell and do not generate electron-hole pairs. Therefore, we can see that the ability to generate electron carriers in the conduction band is a function of the solar cells bandgap energy [Ref. 6:p. 45]. This research used this theory in the selection of the laser wavelength to generate sufficient current within the solar cell. Since wavelength λ is inversely proportional to hv, and the fact that gallium arsenide solar cells, which were used in this study, have an energy gap of 1.4 electron volts, it was determined that a laser had to have a wavelength of less than 885 nm to generate current in the GaAs solar cell.

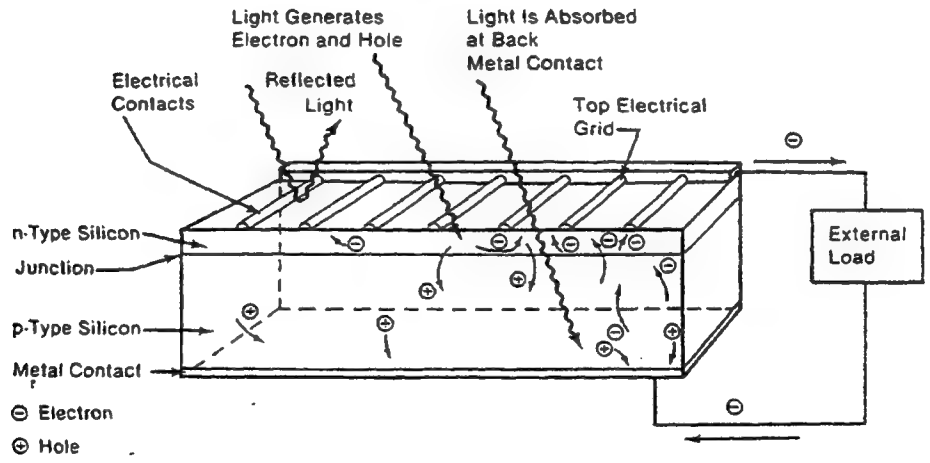

Figure 2-1. Light incident on the cell creates electron-hole pairs, which are separated by the potential barrier, creating a voltage that drives a current through an external circuit.

B. RECOMBINATION AND CARRIER LIFETIME

As discussed above, when photons with an energy level greater than the energy gap of the solar cell strike the cell, electrons may absorb sufficient energy to break their covalent bonds within the crystal lattice structure and be raised to the conduction band, leaving behind an equivalent positive charge, called holes, within the atomic structure. The electron-hole pairs are separated by the p-n junction (also known as the space charge or depletion region) which draws electrons from the p-region to the n-region. Similarly, the holes migrate from the n-region to the p-region. If the holes on the n-side and electrons on the p-side (the minority carriers) are able to diffuse to the edges of the junction before they recombine, which is discussed below, they are swept across the junction. This action creates a photocurrent and voltage difference between the cell terminals and can drive current into the load. [Ref. 1:p. 8]

The collection of photogenerated carriers across the p-n junction is in competition with the loss of these minority carriers by recombination. Recombination is the process which takes place when an electron gives up energy and recombines with a hole before it crosses the depletion region and does not contribute to the generation of current. Recombination can happen by two methods, either (a) directly or (b) indirectly.

Direct recombination is a random process which occurs when the minority carrier (e.g. an electron) interacts with a majority carrier (e.g. a hole). The electron will give up energy and will "recombine" with the hole before it crosses the p-n junction. Indirect recombination occurs when the electron-hole rebonds due to the presence of dangling

bonds from impurities or defects which capture the electrons. The rate at which electrons and holes recombine is

$$Recombination = \frac{n - n_0}{\tau} = \frac{p - p_0}{\tau} (cm^{-3} s^{-1}) \qquad (2.2)$$

where n_0 and p_0 are the electron and hole densities at equilibrium and τ is the lifetime of the carrier [Ref. 6:p. 46]. Long lifetimes are essential for high efficiencies in solar cells. The importance of lifetimes are discussed in greater detail when radiation effects are covered in the next chapter. [Ref. 7p. 27]

C. SPECTRAL RESPONSE

The ability of a solar cell to generate current at a given wavelength is measured by its spectral response. It has been calculated that solar cells are most efficient when illuminated by a monochromatic light source (e.g. a laser) if the wavelength is short enough that it creates electron-hole pairs. However, photons are generally produced by radiation from the Sun. The spectrum for sunlight closely matches that of a 6000 K Black Body Curve. [Ref. 8:p. 45]

The air mass zero (AM0) spectrum in Figure 2-2 [Ref. 8:p. 47] shows the solar spectrum outside the earth's atmosphere with the total incident power integrated over all wavelengths of 1353 watts per m^2 at the Earth's distance from the sun. AM0 will be referred to frequently during this research since it is the standard intensity used when comparing the output parameters of solar cells in space.

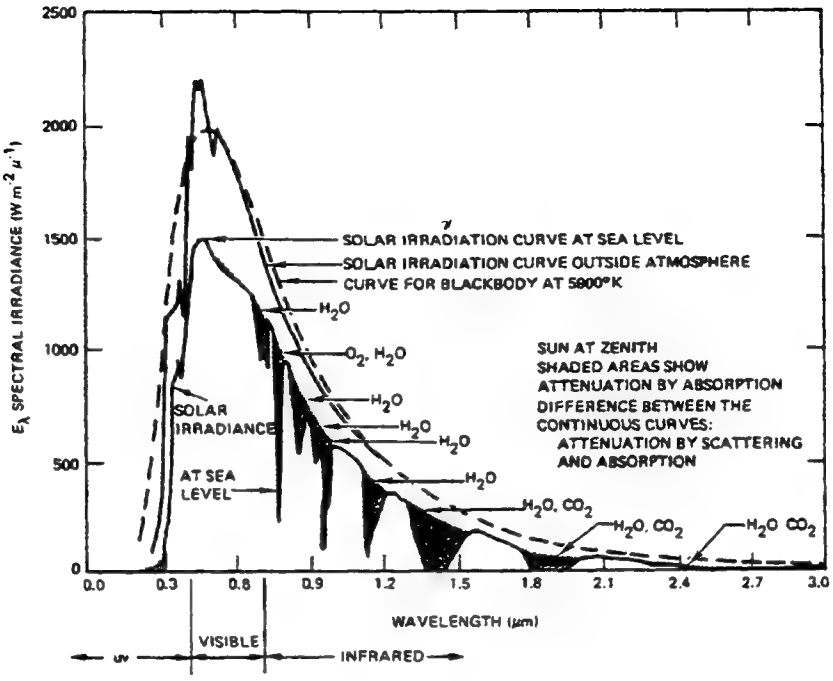

Figure 2-2. Sun Illumination Spectral Irradiance Above the Earth's Atmosphere

D. PARAMETERS

Solar cell behavior is characterized by its current-voltage curve (I-V curve). Most of solar cell's electrical parameters can be extracted from these I-V characteristics.

The solar cell's performance can be can be examined through three main parameters:

1. Open circuit voltage, V_{oc}: This is the voltage output when the cell terminal current is zero.
2. Short circuit current, I_{sc}: This is the current generated by the solar cell when the terminal voltage is zero.
3. Maximum power output point, P_{max}: This is the maximum power produced by the cell. It is the point found on the I-V curve where a rectangle which gives the maximum area can be drawn inside the curve. This point will be found on the "knee" of the curve and is determined by:

$$P_{MAX} = V_M \times I_M \tag{2.3}$$

where V_M and I_M are voltage and current at maximum output points. Figure 2.3 shows an I-V curve of a typical solar cell with the above three parameters shown.

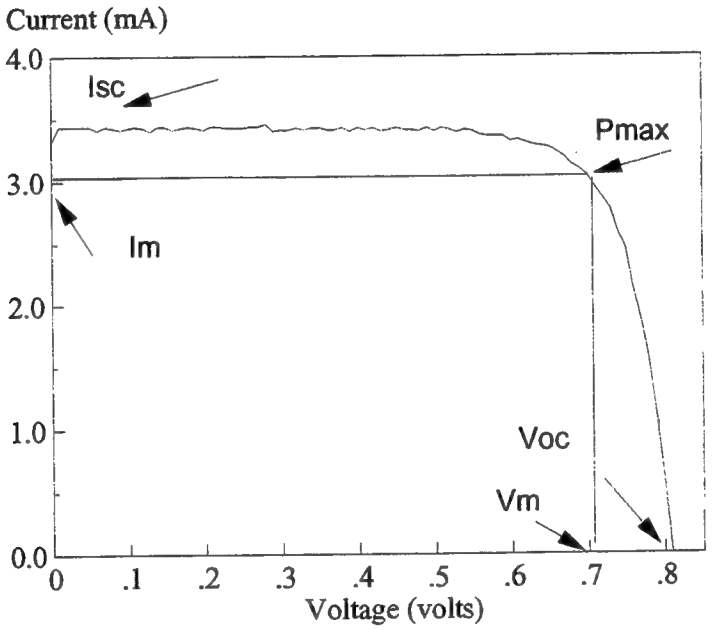

Figure 2-3. I-V Curve of a Solar Cell with Commonly Used Parameters Depicted

Other important parameters that can be calculated from the three extracted parameters are *fill factor* (FF) and *efficiency* of the solar cell.

Fill factor is an indicator of the squareness of the knee. It is the ratio of maximum power out to the product of V_{oc} and I_{sc} and is normally given as a percentage

$$FF = \frac{P_{MAX}}{V_{oc} \times I_{sc}} \times 100 \tag{2.4}$$

The fill factor is a measurement of the quality of the solar cell and is dependent on the cell manufacturing process.

The efficiency of a solar cell is

$$\eta = P_{output}/P_{input} \times 100\%$$

$$\eta = P_{MAX}/(135.3 \times area) \times 100\% \qquad (2.5)$$

where 135.3 mW/cm^2 is the solar constant at Air Mass Zero, AM0, and (area) is the surface area of the cell in square centimeters. This calculates the efficiency of the cell in converting photon energy into electrical energy.

III. RADIATION EFFECTS IN SPACE

Practically all of today's satellites utilize solar cells for power generation. Space research has been evolving for over thirty years. It is not surprising, therefore, that much is now known about the space environment and its adverse effects on solar cells due to particle radiation. It is very complex to analyze the radiation that solar cells encounter in orbit since the type of particle radiation, energy level, and density depend on many other parameters, such as altitude, magnetic latitude, and solar activity. Neglecting neutrons, gamma rays, and alpha particles that contribute very little to the degradation of solar cells because of their relatively weak fluxes, the principal cause of solar cell degradation is due to electron and proton radiation [Ref. 9:p. 641]. Throughout its mission, a spacecraft, encounters continued radiation. The region in space where protons and electrons are trapped above the earth's atmosphere are called the Van Allen belts, and solar arrays of spacecraft within this region experience serious degradation to its power producing capabilities.

A. VAN ALLEN BELTS

The Sun radiates protons and electrons omnidirectionally via the solar wind, its intensity varying with solar flare and sunspot activity. In regions near planets with significant magnetic fields some of these charged particles are trapped and concentrated in radiation belts. The Earth's radiation belts, which trap electrons and protons, are called the Van Allen belts. [Ref. 10:p. 2.2-1]

The shape of the magnetic field is formed by the pressure of the solar wind. The region is compressed on the sunlit side of the Earth and is expanded on the dark side. Charged particles from the Sun are deflected from their original path and tend to follow the lines of force created by the Earth's magnetic field. Particles that are below a critical energy level become trapped and remain in this region. Figure 3-1 [Ref. 18:p. 695] shows the magnetic lines of force that surround the earth and their relative shape. [Ref. 10:p. 2.2-2]

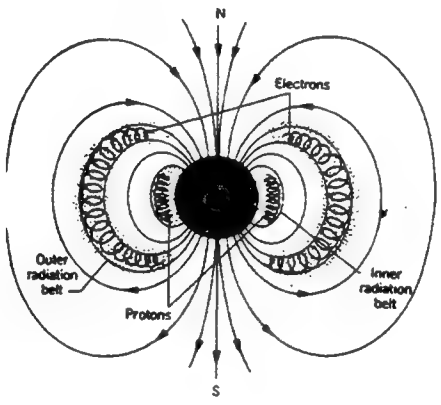

Figure 3-1. The Earth's Magnetic Field, Showing Protons and Electrons Trapped in the Van Allen Radiation Belts

The Earth's magnetic field stretches out into space for many thousands of kilometers. This region is composed of two main belts. The inner belt is located 300-6400 km above the earth and the outer belt is located 13000 km to 59000 km. The inner belt is made up of highly energetic protons (up to 700 MeV) and electrons (20 keV to 1 MeV). The maximum intensity altitude is in the range from 2900 km to 3200 km above the equator.

The outer belt contains electrons with energies from 20 keV to 5 MeV and protons with energy levels greater than 60 MeV. The outer belt reaches two peaks; the first lies between 16000 to 24000 km, while the second is at an altitude of 36000 km. [Ref. 11:p. 2.5-2] Figure 3-2 [Ref. 10:p. 2.2-4] depicts the radiation environment surrounding the Earth.

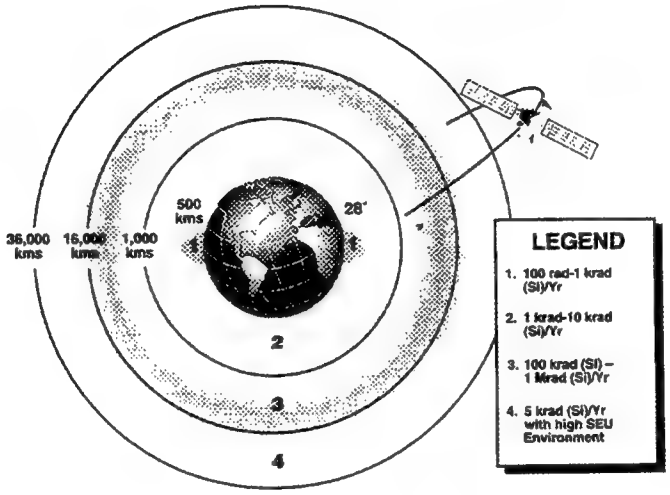

Figure 3-2. Areas of Radiation Outside the Earth's Atmosphere

Electrons and protons may enter the cell through either the coverglass or the substrate [Ref. 11:p. 2.5-3]. The depth of penetration by incident particles depends on the energy level and the wavelength of the particle. The less energetic electron or proton will only damage the surface of the cell, whereas higher energy particles are able to penetrate deeper into the cell's substrate, causing greater damage. [Ref. 2:p. 19]

The mechanical damage to the lattice structure of the cell is created by the ongoing irradiation of the solar cell, causing a gradual deterioration of performance of the cell. The degradation severely affects nearly all solar cell parameters. The following is a list of cell parameters affected [Ref. 11: p. 3.3-1], followed by a graphic representation of these parameters in Figure 3-3:

1. Degradation of short-circuit current of the cell
2. Reduction of the open circuit voltage
3. Decrease in maximum power output
4. Lower energy conversion efficiency
5. Less spectral response of the cell (at longer wavelengths).

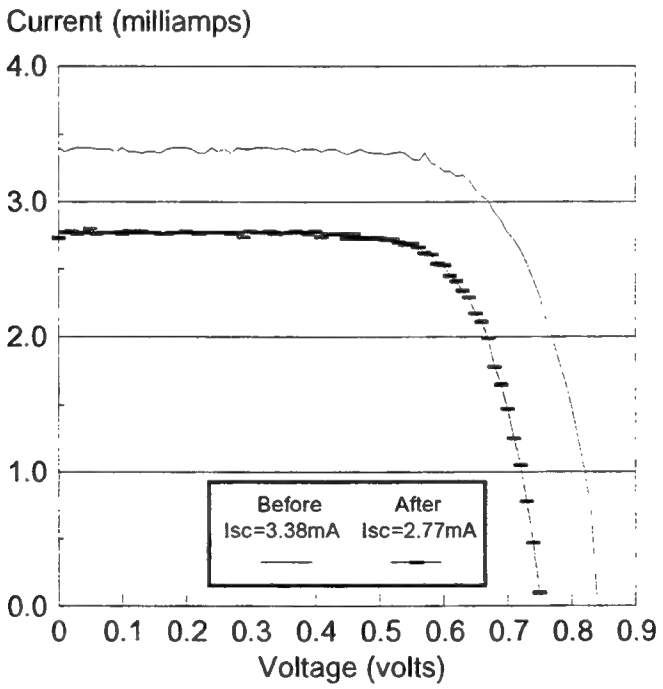

Figure 3-3. The I-V Curve of a Solar Cell Before and After Irradiation with Approximately $1x10^{15}$ e^-/cm^2 of 65 MEV Electrons

B. RADIATION DAMAGE

To operate effectively in the hostile environment within the Van Allen belts, radiation damage must be understood by today's space and electrical engineers in order to minimize its effects.

Radiation defects in solar cells are produced by highly energetic electrons, protons, neutrons, and ions. These fast moving particles have both mass and energy. There are different interactions which occur when these particles bombard solar cells. The dominant interactions are:

1. Inelastic Collisions with Atomic Electrons

This is the case where an energetic particle (i.e., electrons and protons) collides with a bound atomic electron and loses all of its kinetic energy. If the atomic electron receives enough energy, larger than E_g, it becomes free, a process known as atomic ionization. On the other hand, if the radiation particle carries less energy than the material E_g, atomic electrons will become excited without leaving the atom, thus ionization damage will not occur.

2. Elastic Collision with Atomic Nuclei

In this process, an energetic particle will collide with the positive charge of the atomic nucleus and will be electrostatically repulsed from the nucleus. Sometimes enough energy is transferred to the atom to displace it from its lattice position. In most cases the displaced atom would have sufficient energy to displace many other atoms, creating displacement damage.

3. Inelastic Collision with Atomic Nuclei

This is a process during which highly energetic protons collide with the atomic nucleus which excites the nucleus. The nucleus starts to undergo inelastic collisions with large number of neighboring nucleons and the recoiling nucleus is displaced from its lattice site. This nucleus in turn causes more displacements. [Ref. 12:p. 3-2]

Radiation damage resulting in changes in the electrical behavior of the solar cell is divided, in general, into *ionization* and *displacement* damage. The physical damage to a crystal lattice produced by displacement of an atom from its normal lattice position to another location in the lattice is referred to as displacement damage. These displaced atoms then take up interstitial positions or if enough energy has been transferred, knock other atoms from their positions causing ionization and, ultimately, permanent defects within the material. On the other hand, ionization damage takes place by stripping outermost shell electrons of an atom by an incident particle to form ionized atoms and free electrons. [Ref. 12:p. 3-1][Ref. 13:pp. 2-3]

Ionization affects solar cells in several ways. Ionization darkens the solar cell's coverglass. A coverglass is a special transparent shielding material bonded to the surface of the solar cell to protect the cell from heavier radiation particles (namely protons and neutrons). As it darkens, the transmittance of the coverglass is reduced, thereby limiting the effective photons from reaching the cell. Ionizing radiation excites an orbital electron into the conduction band. Impurity atoms present in the coverglass may trap the excited electrons forming color centers. These color centers act to darken the glass reducing the cell's efficiency. [Ref. 7: p. 39]

A beneficial effect of ionization is that it also excites electrons from the valance band to the conduction band creating electron-hole pairs much the same way that carrier pairs are generated by light. However, much more energy is required from ionization radiation to create the carrier pairs. [Ref. 7: p. 39]

Ionization radiation is an inelastic interaction with an atomic electron. If the electron is not sufficiently excited, the electron will not reach the conduction band and will eventually recombine with a hole, transferring its energy into heat thus raising the cell temperature. [Ref. 7:p. 39]

Displacements within the crystal lattice structure of solar cells are caused by highly energetic and fast moving particles. Displaced atoms and their associated vacancies will finally form stable defects within the crystal lattice. Changes in the lattice will alter the equilibrium carrier concentration and the minority carrier lifetime and will affect the cell's efficiency. [Ref. 7:p. 40]

The energy required to displace an atom from its lattice site is on the order of 13 eV for Si and 25 eV for GaAs. [Ref. 7:p. 40]

C. EFFECTS OF LATTICE STRUCTURE DAMAGE

Vacancies, interstitials, and defect clusters in the lattice are also caused by radiation and introduce additional states in the energy gap. These defects may form additional recombination centers which reduces the minority lifetime or they may act as additional impurities which changes the overall impurity composition. These changes in the crystal lattice diminish the solar cell's photovoltaic characteristics. [Ref. 13:p. 157]

D. MINORITY CARRIER LIFETIME

Electron radiation has a significant impact on the minority carrier lifetime. In fact, carrier lifetimes are very sensitive to this type of radiation. As we saw in the previous chapter, the minority carrier lifetime is inversely proportional to the recombination rate of the semiconductor. After the cell has been exposed to electron radiation the lifetime is reduced according to the following relationship

$$1/\tau = 1/\tau_0 + 1/\tau_e \tag{3.1}$$

where

τ = minority carrier lifetime

τ_o= minority carrier lifetime before irradiation

τ_e= minority carrier lifetime due to electron irradiation

Often the above equation is rewritten

$$1/\tau = 1/\tau_0 + \kappa_t \times \theta \tag{3.2}$$

where κ_t is the lifetime damage coefficient and θ is the radiation fluence. [Ref. 14:p. 25]

In theory, the equations above describe why radiation reduces the solar cell's capability in delivering power to the load. Normally, the reduction of performance is not expressed in terms of diffusion length or carrier lifetimes, but rather in terms of the solar cell's I-V curve before and after irradiation. As mentioned earlier, from this curve we

can measure quantitatively the losses by the reduced I_{sc}, V_{oc}, and P_{max} points found on the curve.

IV. DEFECT ANNEALING

Defect annealing is a process which reverses radiation damage that solar cells experience in space. Chapter III described how radiation degrades the electrical power characteristics of a solar cell by damaging the crystal lattice structure of the solid state material. In order to achieve this recovery, atomic restructuring must take place. This can be accomplished by adding heat or driving current through the solar cell which raises the energy level within the cell. The rise in the energy level excites the substrate electrons which recombine with holes that were created by solar radiation. Although the atomic structure of the solid state material will not be completely restored, annealing that does take place will increase the solar cell efficiency and will extend the life of the solar array.

A. ANNEALING PROCESSES

To reverse solar cell degradation, a process of recombination of crystal vacancies and interstitials occur leaving fewer atomic dislocations. That is to say electrons are returned to a bond from which an electron is missing from the crystal's original condition [Ref. 13:p. 197]. Two methods of raising the energy level of the solar cell will be discussed: thermal annealing and minority carrier annealing.

1. Thermal Annealing

There are a number of different ways to anneal radiation damaged solar cells using thermal annealing techniques:

1. Post-annealing
2. Periodic thermal annealing
3. Continuous annealing

Post-annealing is the annealing of solar cells at a given temperature after having been subject to irradiation. Periodic thermal annealing is a process where the cells are irradiated at room temperature (at a lower dose than in the post annealing process), then annealed for a relatively short period of time at a specified temperature. This process is then repeated many times. Continuous annealing is in-situ annealing of the cell while being irradiated. [Ref. 2:pp. 20-22] [Ref. 15:pp. 249-250]

Thermal annealing is by far the most commonly used and the most researched. The application of heat to the solar cell raises the energy level that helps to restore the lattice structure. Recovery of the lattice is proportional to the temperature. Continuous excessive heat also causes the dopants at the p-n junction to diffuse, thus weakening the junction. To successfully anneal the damaged devices, the recovery process must be as rapid as possible so as not to allow a significant migration of dopants from the junction. Generally temperatures above 200°C for GaAs and above 350°C for silicon are considered necessary. [Ref. 14:p. 46]

These high temperatures present certain metallurgical concerns. Presently, solar cell electrical contacts are lead-tin solder (melting temperature of about 190°C) [Ref. 1:p. 161]. The adhesives used to attach the substrate and protective coverglass to the cell begin to fail around 450°C [Ref. 14:p. 47]. If annealing is to become a reality and practical for use in space applications, annealing temperatures must not exceed 150°C.

2. Minority Carrier Injection Annealing

Minority carrier injection current is a technique that creates a very large current density (10 to 100 times greater than the AM0 density) within in the cell. As the current increases, so does the temperature and the minority carrier concentration of the cell (both are appealing effects). Minority carrier injection annealing accelerates the rate of recovery when a forward bias current is applied to the cell's junction at a lower temperature. [Ref. 16:p. 1178] This process can be carried out by two different procedures:

1. Forward bias current injection and
2. By photoinjection

Forward bias current injection uses an external power source to supply a forward bias potential across the solar cell's electrical contacts to force current through the cell. Since the solar cell p-n junction behaves much like that of a diode, an increase in potential across the cell will produce an exponential increase in current through the cell. As the current density is increased in the solar cell a rise in temperature within the cell will also be observed. Ideally, the increase in current will introduce a greater concentration of minority carriers that will become available to reattach themselves to recombination centers that were formed by irradiation. This process will help return the crystal lattice to near pre-irradiation form.

It has been shown in previous work, both at NPS and others, that forward-bias current annealing is successful [Ref. 2:p. 45][Ref. 14:p. 68]. Significant damage recovery to solar cells in the past has proven this technique, but the space applications for

this method might require a separate power supply to induce the results, or through the use of other solar panels as a power source.

This research pursued the idea of minority carrier injection through photoinjection. The theory of photoinjection is to use an intense light source (e.g. 10-100 times more intense than AM0) to produce the required current to induce annealing through the solar cell. The current through the solar cell will respond almost linearly with the intensity of the light source, that is, current will increase proportionally with increase in illumination.

An argon-ion laser was used as a light source in this experiment. This laser is capable of a 500 mW output and produces a visible light beam with a wavelength of approximately 500 nm. The laser wavelength is inversely proportional to the produced light energy which is required to be larger than the solar cell energy gap E_g. This dictates that the wavelength of the laser light has to be shorter than the cutoff wavelength of the cell material in order to produce minority carriers in the material. The intense illumination of the cell will produce a very large current density, which in turn would promote damage recovery in the cell.

As will be discussed in the next chapter, there is much interest in developing lasers for space power applications. The development of lasers dedicated for the sole purpose of power beaming into space could make photoinjection annealing a very practical alternative.

B. PREVIOUS ANNEALING RESEARCH

Research has shown that silicon solar cells with 1 MeV electron damage at fluence doses as high as 10^{16} per square centimeter could be almost entirely recovered by annealing at temperatures of 400° to 450°C in about 20 minutes [Ref. 1:p. 160]. Thermal annealing has been successfully proven in many experiments, but the practicality of annealing at temperatures of 400°C and above is questionable as far as space applications are concerned. It would be difficult and expensive to build the control system for heating and monitoring a solar cell array to such high temperatures for the required periods of time. It would also be somewhat counter productive to generate this amount of energy (produced by the space power system) in order to regain this lost potential.

The use of minority carrier injection has shown that annealing can take place at or near room temperature [Ref. 17:p. 1106]. It has also been discovered that annealing was accelerated when performed at somewhat higher temperatures. Clark demonstrated that a forward bias current and temperatures of 90°-100°C accelerate the annealing process. Clark used a current density of 0.5 amps per cm^2 at 90°C. He found that up to 30% power recovery could be obtained in 48 hours. [Ref. 14:p. 68]

Cypranowski also proved that solar cells could recover 90 percent or better of their lost capability after repetitive cycles of irradiating followed by annealing. Here too, the best results were with a current density of 0.5 amps per cm^2 and temperatures between 90°C and 100°C. [Ref. 2:p. 45]

V. LASERS

Even though lasers have only been around for approximately thirty years, they have become a major player in medical, electrical, communication, and military fields. Lasers have become so prevalent that they are even found in the checkout counter (bar code reader) at the grocery store. Today's technology is finding more uses for lasers than ever imagined.

There have been significant advances made concerning lasers, optics, and solar cells that may make it possible to power space satellites with ground-based lasers. [Ref. 3:pp. 3-6][Ref. 4:p. 4] The potential applications listed in these references include:

1. Power space craft during eclipses
2. Enhance electric thruster capability to make orbital transfers and station keeping more efficient
3. Replacing/reducing the alternate power supply, or batteries, by using lasers when required

with advantages of :

1. Less batteries required
2. Less propellant
3. Greater solar cell efficiency
4. Lower launch weight

The focus of this research is to explore the possible option of using lasers to induce the annealing process in damaged solar cells.

To fully appreciate the importance of lasers and why they have become so valuable, this chapter will review some of their characteristics and potential space applications.

A. DEFINITIONS

Laser is an acronym for Light Amplification by the Stimulated Emission of Radiation. As the name implies, laser operation has to do with stimulated emission of energy. However, before the operation of the laser and its characteristics are discussed, some definitions should first be introduced [Ref. 18:p. 1041]:

1. Absorption

This takes place when a photon interacts with an atom and loses its energy to that atom. The excited atom will move into an upper energy state.

2. Spontaneous Emission

When an atom is in an upper energy state, E_2, with no radiation present, this atom will eventually move to a lower energy level, E_1, emitting a photon of energy $h\nu$ in the process.

$$h\nu = E_2 - E_1 \tag{5.1}$$

The mean life time of an excited atom is about 10^{-8} seconds. Some states however, have a much longer lifetime, approaching as long as 10^{-3} seconds. The states with a longer mean life time are called metastable states and are what allows lasing to be produced.

3. Stimulated Emission

This situation occurs when an atom is in an upper energy state and radiation is present (e.g. a light source) and it interacts with a radiative photon. The result is that the atom moves to its lower energy state, producing a second photon.

4. Population inversion

In order to generate light from a laser there must be more atoms in the upper energy level than in the lower energy level. This is called population inversion.

B. LASER LIGHT

The unique properties of laser light are caused by a chain reaction of stimulated emissions events that occur within a "lasing" medium (e.g. Argon-ion as used in this research). Lasing always involves a pair of energy states, E_1 and E_2. For stimulated emission to be the dominant process there are two requirements. First, the higher energy level E_2, must contain more atoms than the lower energy level E_1, in other words a population inversion exists between E_1 and E_2. Secondly, the upper level must have a relatively long mean lifetime against depletion due to spontaneous emission. [Ref. 18:p. 1046]

Population inversion must be induced since it breaks the law of thermal equilibrium. This is done by either supplying enough energy to the system so that many atoms are raised to an excited state (optical pumping), or by a special gas mixture where collisions between the atoms elevate the lasing medium atoms to the higher level. [Ref. 18:pp. 1041-1043]

The gas collision excitation process will be briefly explained with a three-energy-level model. Pumping is accomplished by setting up an electrically induced gas discharge in the lasing medium. Electrons and ions collide frequently enough to raise the lasing atoms to an upper energy level E_3. From state E_3 many atoms rapidly decay to state E_2 which, if lasing is to be produced, must be a metastable level so that spontaneous emission to the ground state occurs very slowly and this results in a population inversion. A photon of the right energy that interacts with E_2 can trigger an avalanche of stimulated emissions from state E_2. The light that is generated will be of the wavelength of the lasing medium (e.g. 632.8 nm for neon). The mirror optics within the resonant cavity will not be discussed. [Ref. 18:p. 1043]

C. ARGON -ION LASER

A 500 mW laser was used for this research to anneal solar cells. This laser produces laser light in the visible spectrum with a wavelength between 475 to 514 nm. The excitation mechanism involves collisions between argon-ions and energetic electrons. The pumping is achieved by multiple collisions of Argon ground state ions and electrons followed by a number of cascading paths. The energy levels of an Argon-ion laser are depicted in Figure 5-1. [Ref. 19:pp. 244-245]

D. LASER CHARACTERISTICS

The premise of this research is based on laser characteristics and their potential use to illuminate solar cells. The laser has many unique qualities which are very attractive

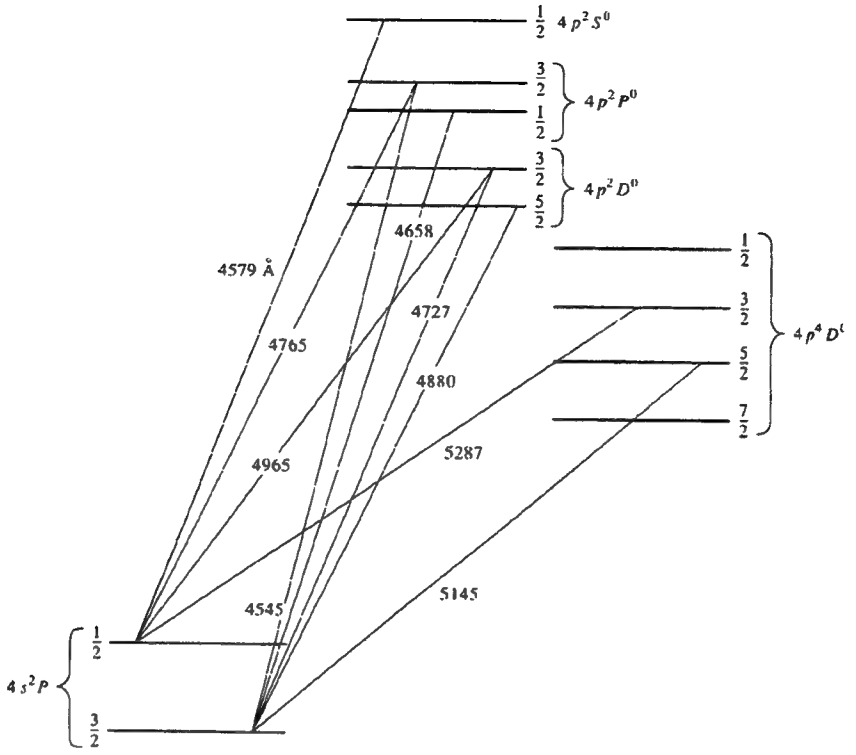

Figure 5-1. Energy Levels of an Argon-ion Laser Transitions

when considering their application with respect to solar cells. Some of the characteristics which apply to this research are:

1. Laser light is highly monochromatic, narrow in frequency or wavelength spectrum
2. Laser light is highly coherent
3. Laser light is highly directional
4. Laser light can be sharply focused

Lasers produce a very narrow, intense beam and as will be discussed, solar cells are more efficient under laser illumination.

E. SOLAR CELL PERFORMANCE UNDER LASER ILLUMINATION

Solar cell efficiency is dramatically increased using a monochromatic light source if the wavelength of the source is in the visible spectrum. The most commonly used solar

cells have their best response to monochromatic illumination at about 850 nm for GaAs cells and about 950 nm for Si cells [Ref. 3:p. 1496]. For shorter wavelengths, efficiency will fall off linearly with wavelength. Though at these shorter wavelengths, the solar cell will produce power, much of the energy in the lower end of the spectrum will be given off as heat. As the wavelength becomes longer, solar cell efficiency rapidly drops to zero. There is little or no response for wavelengths longer than the cutoff wavelength λ_c or in other words, at energies lower than the bandgap energy of the cell material. As seen in equation 5.2 which is derived from equation 2.1, the maximum wavelength is determined by the energy gap of the solar cell material:

$$\lambda_c = \frac{1.24}{E_g} \tag{5.2}$$

where E_g is the bandgap energy in electron volts.

The response of a solar cell to monochromatic light is much higher in terms of efficiency than that produced by the solar spectrum. For conventional Silicon and Gallium Arsenide cells under AM0 conditions, the highest achieved efficiencies are 18 and 22 percent for Si and GaAs, respectively. However, under laser illumination GaAs efficiency can reach over 50 percent and Si cells can reach over 40 percent. [Ref. 3:p. 1499]

F. LASER SYSTEMS

Lasers that are to be considered for solar cell applications must operate within the visible spectrum where the atmosphere is nearly transparent to their transmission. It has

been determined that the minimum wavelength is about 350 nm because of atmospheric scattering. The maximum wavelength is set by the response of the solar cells, or about 850 nm for GaAs or 950 nm for Si as previously mentioned. [Ref. 3:p. 1496]

Several types of lasers are available for space applications. Free electron lasers have a power output in the megawatt range and can be tuned to provide optimum wavelengths for both solar cells and atmospheric transmission. Currently, there is a free electron laser that is under construction that will be capable of transmitting light with a wavelength in the range of 850 nm. [Ref. 3:p. 1496]

G. PREVIOUS ANNEALING RESEARCH WITH LASERS

A Copper-Halide laser had been used to significantly anneal a radiation damaged silicon solar cell. The procedure used a high power pulsed laser with a peak pulse power of 75 kW/cm^2 at a 511 nm wavelength. The solar cells had been irradiated with 1 MeV to an electron fluence 10^{15} electrons/cm^2. [Ref. 5:pp. 277-279]

In this research, the laser was focused to a spot size of 0.17 cm then the beam was mechanically swept back and forth across a Si cell, slowly advancing at a rate of 0.13 cm/sec for an energy density of about 500 j/cm^2 on the cell surface. The electron radiation degraded the cell 17%, in terms of short circuit current. After the annealing process, the Si cell recovered to 88% of initial capability for a gain of 5%.

This annealing process used the laser as an intense source for heating the cell to an extremely high temperature to induce thermal annealing. Past researchers conducted similar annealing work with good results [Ref. 20 and Ref. 21].

Again, the practicality of using a laser in this method is questionable with today's technology. The laser power required to produce such high heat on an orbiting satellite is order of magnitudes larger than even the proposed high power lasers that are being investigated for power beaming. This does not take into account all other problems that might arise by heating the satellite to such extreme temperatures, as discussed in the previous chapter.

No references were found that used lasers to anneal solar cells through the process of photo-injection, the method used in this research.

VI. NPS LINEAR ACCELERATOR

The NPS Linear accelerator (LINAC) was used to simulate the electron radiation environment that solar cells are exposed to in space while orbiting the Earth. The LINAC is a traveling wave type linear accelerator which has three ten foot long accelerator sections (waveguides), each powered by a twenty-two megawatt Klystron amplifier. The LINAC uses an electron gun to inject electrons into the first of three sections of the accelerator. The "gun" is a cathodic grid that produces pulses of narrow circular beams of electrons. These electrons are energized and are accelerated through the three separate stages by their applied radio frequency (RF) fields. The RF energy is produced by a Klystron amplifier located at the entrance of each section.

The electrons start with an energy of around 80 keV when they are injected into the waveguide from the gun. The electron beam is steered (by magnets) 45° off of the acceleration axis and enters the target area. After exiting from the last section, the electrons are focused onto the target by two quadrapole magnets that are located directly prior to the primary chamber. The magnets are able to focus the beam anywhere from a spot with a 4 mm diameter up to an area of 5 cm^2. [Ref. 22:pp. 11-24][Ref. 23:pp 42-43]

To observe the electron beam from the control room, the target is painted with phosphorous material, which becomes florescent by the incident electrons. This process is monitored by a closed circuit television system whose signal is transmitted to the control room. In this research the beam was focused to a 1.27 cm diameter spot at the rear of the secondary chamber then a filter was placed in the primary chamber which

expanded the beam to approximately a 2.8 centimeter diameter beam in the secondary chamber. This beam size was sufficient in order to expose the five test cells to the electron radiation at the same time.

The number of electrons that irradiate the cell, or the fluence, is measured through the use of a Secondary Emissions Monitor (SEM) located at the rear of the target chamber. As the electron beam passes through the SEM, it causes a charge to accumulate on a capacitor. The capacitor is connected to digital voltage integrator in the control room. The total charge accumulated on the capacitor is determined by using the relationship

$$Q = C \times V \tag{6.1}$$

where Q represents the total charge, C is the value of the capacitor, and V is the measured voltage across the capacitor. Since we know that

$$Q = n \times q \tag{6.2}$$

where q is the charge per electron and n is the total number of electrons. Then the theoretical number of electrons that are passed through the SEM can be calculated as

$$n = (C \times V) \div q \tag{6.3}$$

Previous work done using the NPS LINAC has shown that the SEM is only 10% efficient

in its electron collection process. Therefore, the total number of electrons can be expressed as

$$n = (C \times V) \div (q \times .1) \tag{6.4}$$

It is the usual custom to discuss the amount of irradiation that solar cells receive in terms of beam fluence which is the number of particles per unit area as shown below

$$\Phi = n \div (BeamArea) = C \times V \div (.1 \times q \times A) \tag{6.5}$$

Figure 6.1 depicts the layout of the NPS linear accelerator, used in this research [Ref. 23:p. 44].

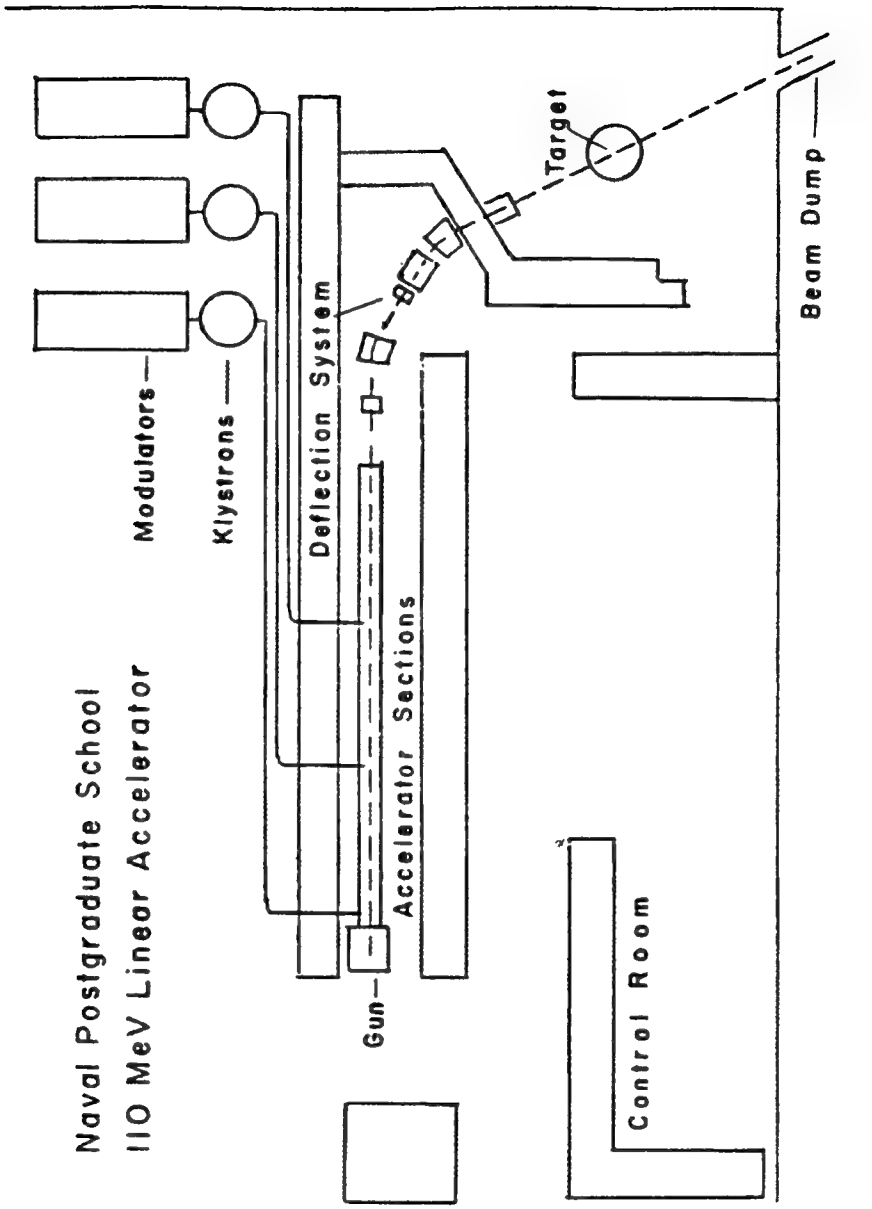

Figure 6-1. NPS LINAC Configuration

VII. EXPERIMENTAL PROCEDURES

A general outline of the experimental procedure may be divided into two parts: 1) irradiation of cells using the LINAC, and 2) laser annealing, with I-V curves of the cells obtained before and after each part.

The I-V curve for each cell was obtained using a solar simulator utilizing a Xenon lamp to obtain an illumination corresponding to Air Mass Zero where the solar intensity is equal to 1353 W/cm^2. The process is performed before and after each cell received irradiation from the NPS LINAC. The curves were used to verify the amount of radiation fluence the cells were exposed to, and to determine the level of annealing or recovery that laser light induced. A silicon standard cell was used to verify the calibration of the solar simulator.

A. THE NPS SOLAR SIMULATOR SETUP

The solar simulator used in this research was the SS-1000 manufactured by Optical Radiation Corporation. In addition to the solar simulator, the solar simulation system consisted of five other major components. These were the Hewlett Packard 6626A programmable power supply, an IBM PC/XT computer, an HP-IB interface, a standard cell mounted on a brass holder, and a temperature-controlled water circulator which circulated water through the brass holder to maintain a constant test cell temperature during the I-V measurements.

The SS-1000 simulator uses a xenon bulb that produces a black body spectrum which, as mentioned previously, closely matches the solar light spectrum in space. The intensity of the light and beam uniformity has to be adjusted using three focus adjustments that control the X, Y, and Z positioning of the lamp. To verify the uniformity of the beam, a grid was centered under the light over which a calibrated cell was placed to measure light intensity. Once this alignment was accomplished, only minor vertical movement of the lamp using the Z axis adjustment was necessary to compensate for small changes in beam intensity.

The standard cell used was a Silicon K6700A solar cell received from the Jet Propulsion Laboratories. Documentation of a standard cell included V_{oc}, I_{sc}, P_{max}, and the I-V curve of the cell under AM0 conditions. Figure 7-1 shows the cell's corresponding I-V curve and Table 7.1 summarizes the specifications of the standard

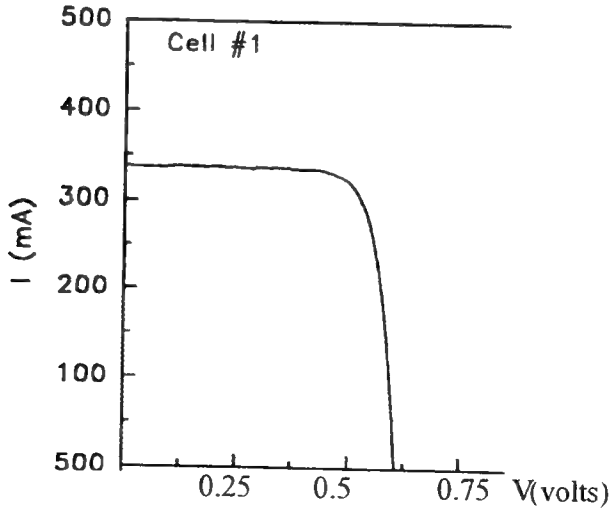

Figure 7-1. I-V Curve of Standard Cell

cell. Detailed specification sheet and data of the standard solar cell are included in Appendix A.

TABLE 7.1. SPECIFICATION DATA FOR STANDARD CELL AT AM0

Cell Size	I_{sc} (mA)	V_{oc} (V)	P_{max} (mW)
7.68 cm^2	338.264	0.6063	161.411

To ensure that the solar simulator was properly adjusted so that the intensity of illumination at the test site was at 1353W/m^2, or AM0. The calibrated cell was placed under the solar simulator before the simulator light intensity level was adjusted while simultaneously measuring the cell's short circuit current and open circuit voltage with a multimeter. Once the solar simulator was finely tuned to match the cell's specification data sheet, an I-V curve was generated and the data recorded in order to, again, compare with the manufacturer calibrated specifications. This was a tedious procedure because light illumination from the simulator varied somewhat with time. Variation of the intensity is usually confined to a few milliwatt fluctuation in the calibrated cell's output. However, since this research used much smaller cells (4 mm diameter GaAs cells), the fluctuation could have a great impact on the data due to the small output of the cell. To police the simulator variation, calibration checks were conducted before and after each test cell curve was obtained.

I-V curves for each test cell were produced under AM0 conditions before and after electron irradiation so as to quantify the radiation damage.

The I-V curves were plotted through the use of the HP programmable power supply, the HP-IB card, and the PC/XT computer. No past work had used this HP programmable power supply with the new SS-1000 solar simulator to conduct calibrated solar cell testing. Though NPS had a previous solar simulator laboratory, it had been upgraded to incorporate testing for the Petite Amateur Navy Satellite (PANSAT) program.

Pre-experimental trials were conducted using this setup to ensure an accurate measurement of solar cell characteristics for both the calibration cell and test cells. The power supply was used to both sink and source current to the solar cell. The HP-IB board provided the interface for remote programmable operation between the computer and the power supply. The program increased the power supply output in .01 volt increments. The power supply measured and processed output current of each cell and the data was recorded by the PC at each interval. The manufacturer specifications for the power supply are included Appendix B.

To maintain the cell temperature during testing, the calibrated cell was mounted on a brass block using a space certified adhesive for space power systems. The brass block was kept water-cooled to maintain a temperature of 28°C ± 2°C. A thermocouple was mounted on the cell so that the temperature of the cell could be monitored separately from the water temperature.

Leads were then soldered onto the calibrated cell, then the cell was wired in series with the HP power supply as a load. When the cell is illuminated by light, as shown in Figure 7-2, the cell generated current is sunk into the power supply. The power supply was programmed to step up a load voltage incrementally from 0 volts, which corresponds

to short circuit current I_{sc}, to the point where the load creates a virtual open circuit V_{oc}. The voltage increments determine the resolution of the curve and therefore the accuracy of the fill factor and maximum power point.

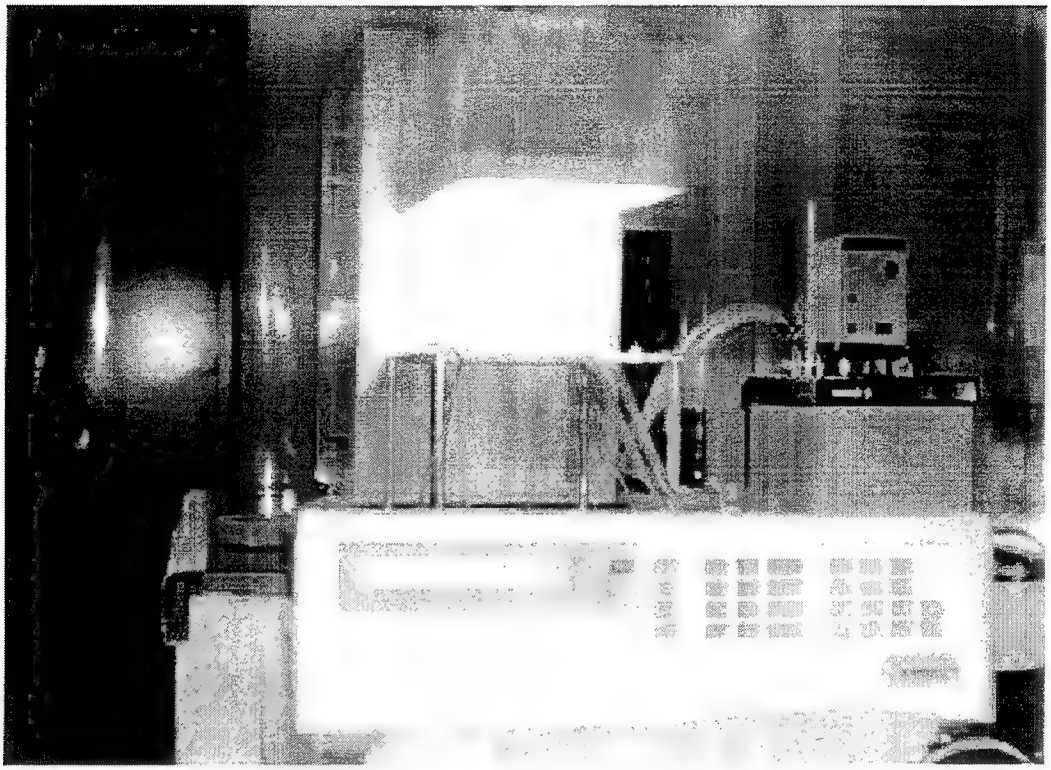

Figure 7-2. The Standard Cell Illuminated by the Solar Simulator

A pre-existing program for another power supply had to be modified so that the HP power supply would maintain a regulated output. The program was further modified for proper voltage resolution, data output, data recovery, and proper scaling. The BASIC program is included in Appendix C.

As the cell is being illuminated, the data measured by the power supply is recorded by the computer and the I-V curve is plotted simultaneously on the monitor, Figure 7-3.

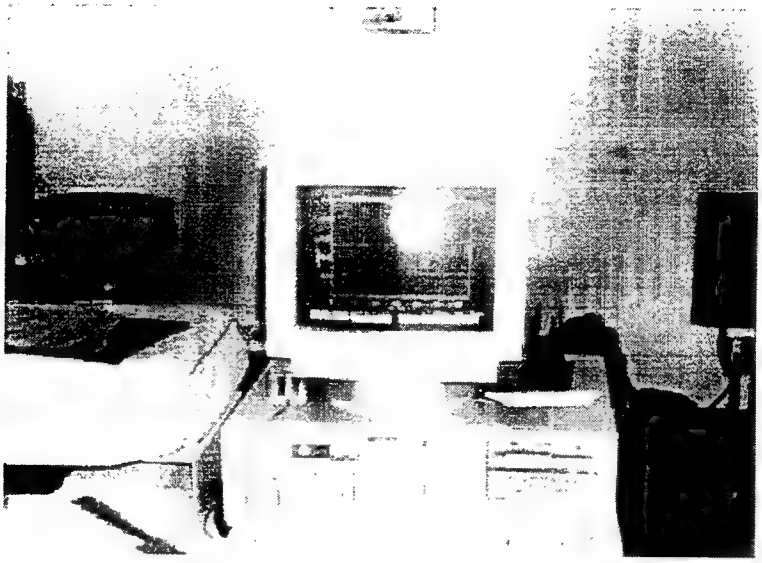

Figure 7-3. Data is Sent to the Computer and Plotted on the Monitor

Data sent to memory could then be used to determine cell efficiency, P_{max}, I_{sc}, and V_{oc}. Figures 7-4 and 7-5 shows the system configuration and equivalent circuit, respectively.

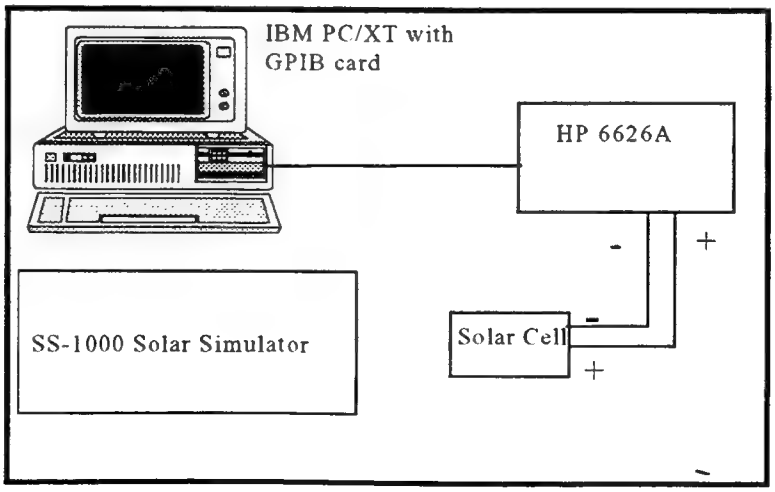

Figure 7-4. The System Configuration of the Solar Simulator System

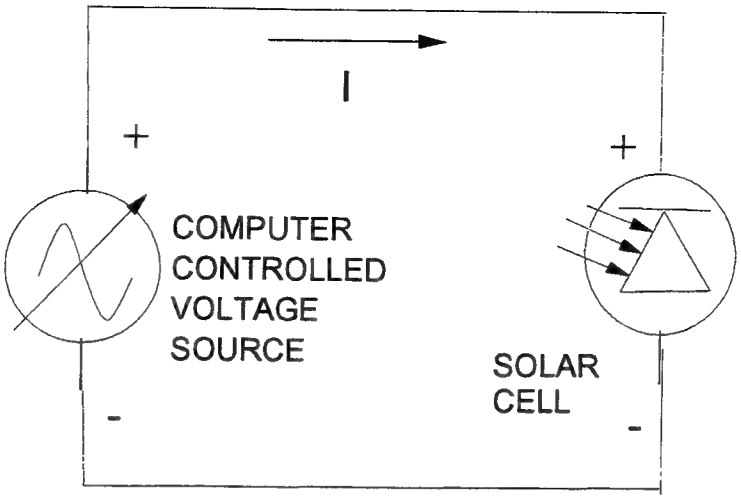

Figure 7-5. Equivalent Circuit

Following the above procedure, I-V curves were generated for six 4 mm diameter GaAs test solar cells, as well as two 2x2 cm^2 GaAs solar cells that were used to verify the fluence of radiation of the linear accelerator before irradiating the test cells with the LINAC.

B. THE SOLAR CELLS USED IN THE RESEARCH

Six relatively small (4 mm diameter) GaAs solar cells were chosen as the test cells for this research. The cells had been purchased from Applied Solar Energy Corporation (ASEC) in 1987. Due to their small size, these cells were considered ideal for this experiment since the laser was capable of illuminating the entire solar cell area without the aide of optics to expand the beam. One cell was not irradiated and was used in conjunction with the standard cell as an additional standard for AM0 measurements.

C. IRRADIATION PROCEDURES

Three runs were conducted using the LINAC. The first run conducted was to study the fluence distribution of the electron beam. If focused properly, the normal beam distribution of the LINAC is Gaussian in shape. To verify this, the accelerator was run to analyze the electron beam. Using a Macintosh II computer, loaded with a software package which included *Image* software, and video cameras, an image of the electron beam was captured and digitized for display on the computer screen. The pixel intensities ranged from 0 (white) to 255 (black). Figure 7-6 shows a line intensity profile of the electron beam. As can be seen, the density profile is Guassian in nature so the distribution of the electron beam could be obtained. More importantly, when the five GaAs cell were irradiated, they did not all receive the same fluence level, rather, they received varying amounts of radiation with the maximum at approximately $1x10^{15}$ electron fluence.

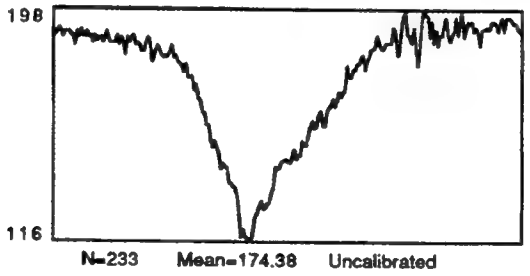

7-6. Density Profile Plot of the LINAC Electron Beam

Previous data has shown that an electron fluence of 1×10^{15} electrons/cm^2 produces power degradation of up to 20-30% of solar cell output power. Such degradation would

be apparent when comparing current-voltage curves and would allow identification/recognition of cell recovery after the annealing process. The equations discussed in the Linear Accelerator chapter were used to determine the amount of time needed to run the LINAC in order to accumulate the required electron fluence:

$$V = (n \times q \times .1) \div C \tag{7.1}$$

where the capacitor value used was .1μF and the SEM efficiency was 10%. This results in:

$$V = (10^{15} \times (1.6 \times 10^{-19}) \times .1) \div (0.1 \times 10^{-6}) = 160 Volts \tag{7.2}$$

When 160 volts had accumulated on the capacitor shunted across the Secondary Emissions Monitor (SEM) of the LINAC then $1x10^{15}$ electrons had theoretically passed through the target.

To verify that these equations would be of adequate accuracy, a second test was performed to irradiate a 2x2 cm^2 GaAs solar cell. Cell #1 was used to conduct this experiment and was placed under LINAC illumination electron beam, as displayed in Figure 7-7. The LINAC beam is monitored remotely from the control room by a closed circuit television system and using the *Image* software mentioned previously. As can be seen from Figure 7-7, the beam illuminates the phosphorous screen around the target cell. The beam is focused by two quadrapole magnets that steer the beam onto the target.

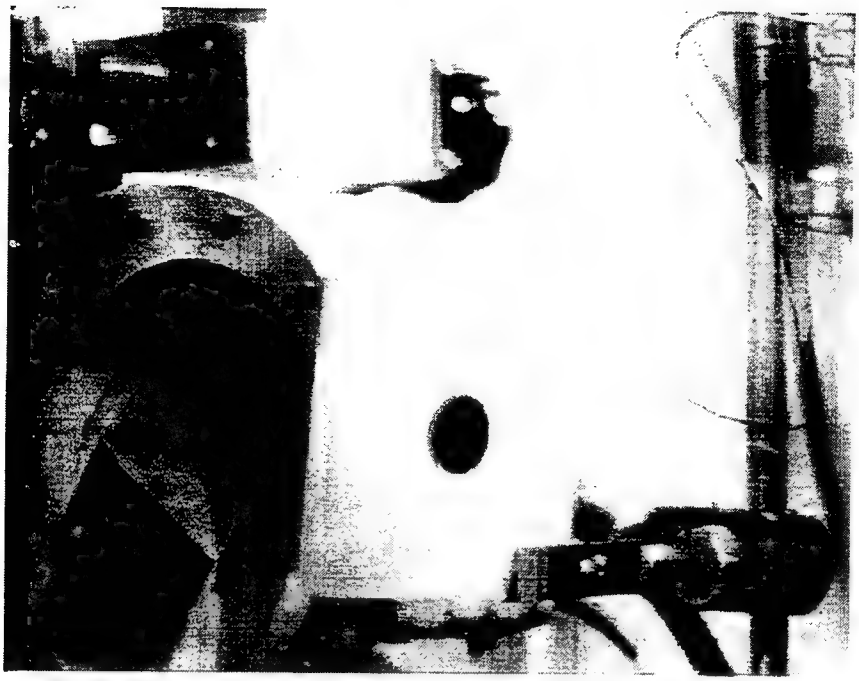

Figure 7-7. Solar Cell #1 Under LINAC Electron Beam

Following the irradiation, another I-V curve was generated on cell #1, as shown in Figure 7-8. From Figure 7-8, the short-circuit current at AM0 of cell #1 was found to be approximately 0.9 Amps, down from approximately 0.113 Amps before irradiation. This corresponds to a degradation of about 20 percent. Using Figure 7-9 [Ref. 12:p. 3-148], which shows normalized short circuit current curves vs. electron fluence, the percent degradation at 10^{15} electrons/cm^2 is just under 85%--or a degradation of just over 15%. This verified the LINAC equations to be fairly accurate. The 5% difference was attributed to the fact the LINAC produced a 65 MeV electron beam whereas Figure 7-9 is associated with a 1 MeV equivalence.

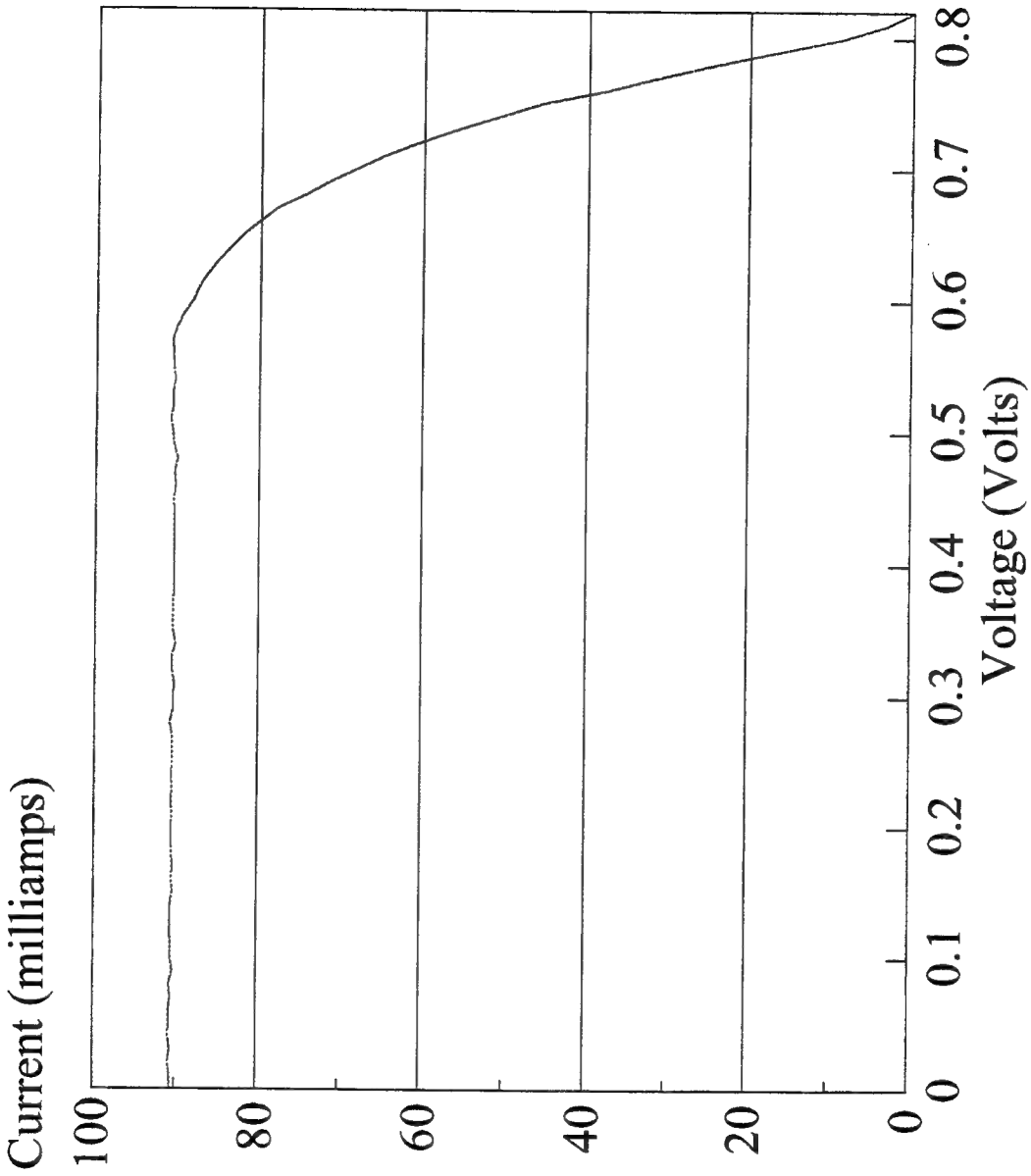

Figure 7-8. I-V Curve of Cell #1 After Irradiation by LINAC

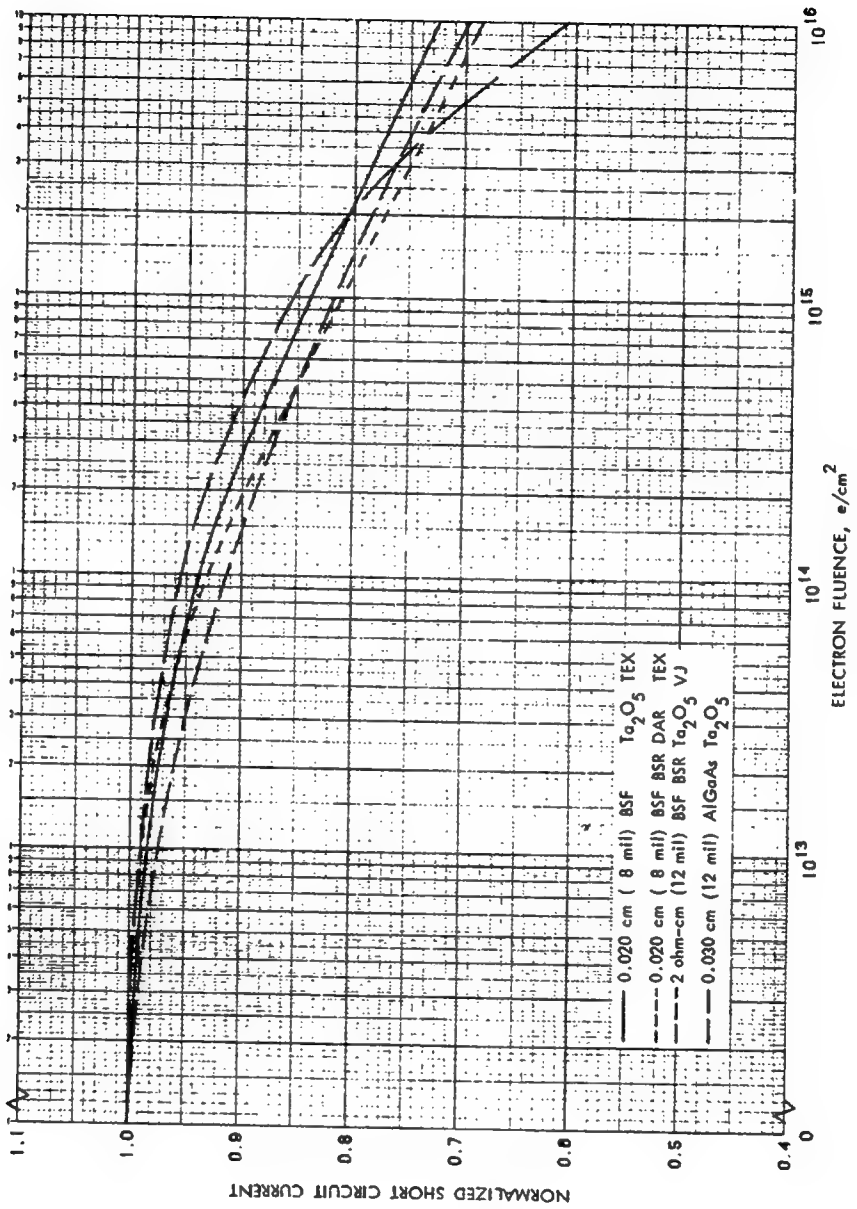

Figure 7-9. Normalized I_{sc} vs 1 MeV Electron Fluence for Si and AlGaAs Cells

The third and final run of the linear accelerator was conducted on the five GaAs test cells. These cells were labeled A, B, D, E and F (cell C was reserved for reference in determining AM0 under the solar simulator). As shown in Figure 7-10, these cells were placed in a semi-circle distribution with cell F closest to the center.

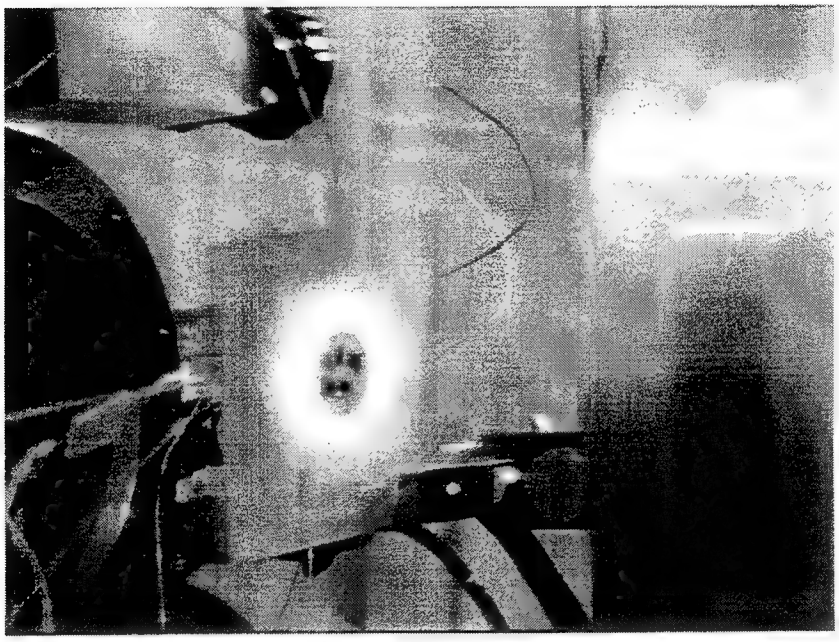

Figure 7-10. Irradiation of 5 GaAs Test Cells with the LINAC Electron Beam

D. ANNEALING PROCEDURES

In earlier work, annealing took place in GaAs solar cells with forward bias current and heat applied to the cell, creating a current density of 0.5 amps/cm^2 and at cell temperature of 90-100°C. The intent of this work was two-fold: 1) to show that a laser could produce enough self-generated current within a solar cell to create a similar current

density and 2) that the laser would also increase the cell temperature, where the other methods required an external heater.

To obtain a current density of at least 0.5 amps/cm^2 through a cell with an area of 12.6 mm^2, the laser beam had to be expanded to cover the surface area of the cell and provide enough power to generate 60 milliamps of current out of the solar cell. From earlier procedures it had been determined that the test cells produced 3.2 to 3.5 milliamps of current under AM0, therefore, the laser beam power had to an equivalent of 20 times AM0. This required a laser that could produce at least 310 milliwatts.

To further simulate the space environment, the solar cells were heated to a temperature that is consistent with the steady state temperature under illumination from the sun. Table 7.3 shows, temperature variation of a sun-oriented flat array as a function of altitude from 370 km to geosynchronous altitude [Ref. 10:p. 8.5-4].

TABLE 7.2. FLAT SOLAR PANE TEMPERATURE VARIATION AS A FUNCTION OF ORBIT ALTITUDE

Circular Orbit Altitude (km)	Solar Panel Steady-State Temperature (°C)	Circular Orbit Altitude (km)	Solar Panel Steady-State Temperature (°C)
370	67	7,410	57
740	65	14,820	55
1,110	64	22,240	54
1,850	62	35,880	53

An average cell temperature of 60°C was chosen. The cell was mounted on a 1ohm resistor, that had approximately 1.5 Amps of current through it, such that the power dissipation would cause the cell temperature to reach 60 °C. Once the solar cell had reached a steady state temperature, the argon-ion laser beam was focused on the cell. The cell was wired in a short circuit configuration. At regular intervals, the cell's output current was measured with a multimeter and the temperature of the cell was recorded. Thermocouples were attached to each of the five cells so that annealing temperatures could be recorded. Figure 7-11 shows the layout of the laser, with the test cell mounted on the resistor that is placed under the fiber optic cable.

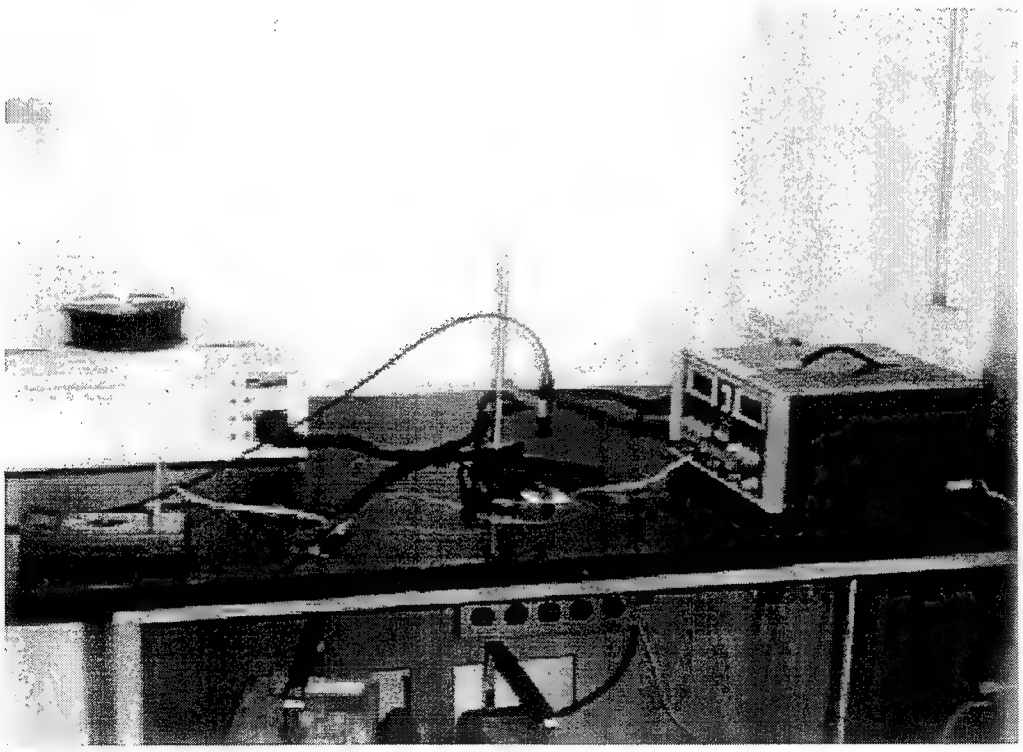

Figure 7-11. The Annealing Process Required the Solar Cell to be Illuminated by the Laser and was Placed Beneath an 8 Foot Fiber Optic Cable

As can be seen from Figure 7-11, a fiber optic cable was used to expand and focus the output of the laser. Some power losses were expected in the beam power so, a 500 milliwatt laser with a visible wavelength (Argon-ion laser produces a 475-514 nm wavelength) was used to ensure illumination of 20 x AM0 intensity.

VIII. RESULTS

Analysis of the five test cells following irradiation by the LINAC revealed that they had received varying amounts of radiation, due to the Guassian shape of the electron beam, as expected. Table 8.1 tabulates the changes in I_{sc}, V_{oc}, and P_{max} after being exposed to electron radiation and an estimate of the electron fluence each cell received is shown in Table 8.2. The data in Table 8.2 was determined by averaging the equivalent 1MeV fluence found in Figures 7-9 and 8-1. The I-V and P_{max} curves of the five cells, before and after irradiation, are given in Appendix D.

TABLE 8.1. PARAMETERS OF CELLS BEFORE AND AFTER IRRADIATION

	V_{oc} (Volts)		I_{sc} (Amps)		P_{max} (mW)	
	Before	After	Before	After	Before	After
Cell A	0.84	0.75	3.38	2.77	2.02	1.52
Cell B	0.83	0.77	3.33	2.92	2.06	1.67
Cell D	0.8	0.76	3.42	2.88	2.14	1.68
Cell E	0.81	0.75	3.32	2.77	2.03	1.53
Cell F	0.85	0.78	3.11	2.6	1.97	1.52

TABLE 8.2. CALCULATED EQUIVALENT 1MeV FLUENCE

	Normalized Power	Normalized I_{sc}	Estimated Φ
Cell A	0.75	0.82	1.8×10^{15} (e/cm^2)
Cell B	0.81	0.88	8.5×10^{14} (e/cm^2)
Cell D	0.79	0.84	1.2×10^{15} (e/cm^2)
Cell E	0.76	0.83	1.6×10^{15} (e/cm^2)
Cell F	0.78	0.84	1.4×10^{15} (e/cm^2)

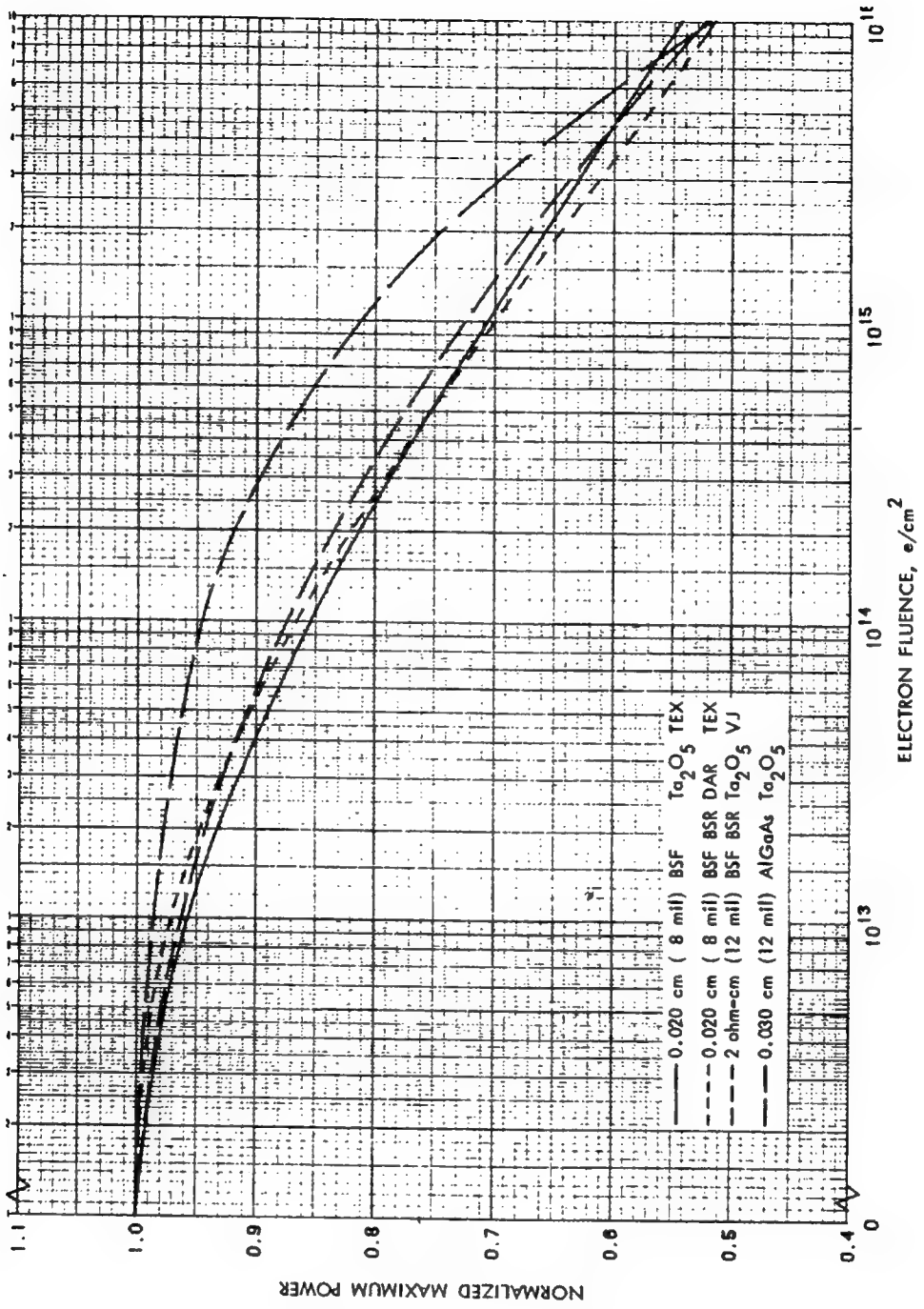

Figure 8-1. Normalized P_{max} vs. 1 MeV Electron Fluence

The calculated fluence was less than the actual dose received. The electron beam that irradiated the five cells had a diameter of 3.6 centimeters and, by using equation 6-6, the calculated dose was found to be 1 x 10^{14} electrons/cm^2. As previously stated, the difference in the calculated and estimated electron fluence is attributed to the fact that a 65 MeV electron beam was used vice a 1 MeV (due to the limitations of the NPS LINAC). Figures 7.9 and 8.1 [Ref. 12:p. 3-23] use 1 MeV fluence to estimate solar cell degradation. As can be seen in Figure 8.2, more degradation to cell parameters occur at higher electron energy levels.

Once the laser annealing procedures had begun, the cells were removed from under the laser and I-V curves were plotted at various time intervals to determine if there was any discernible annealing. If annealing had taken place, the process was stopped and the next cell was tested. None of the cells were annealed for longer than 24 hours. Table 8.3 gives the total annealing time and the percent of the recovered degradation by annealing with an Argon-ion laser. Post-anneal I-V curves of the test cells are shown in Appendix D.

TABLE 8.3. THE PERCENT INCREASE IN BOTH SHORT CIRCUIT CURRENT AND MAXIMUM POWER POINTS AFTER ANNEALING

	Cell A	Cell B	Cell D	Cell E	Cell F
I_{sc}	16	24	15	13	0
P_{max}	0	28	9	19	0
Time	16Hrs.	24Hrs.	24Hrs.	20 Hrs.	18 Hrs.

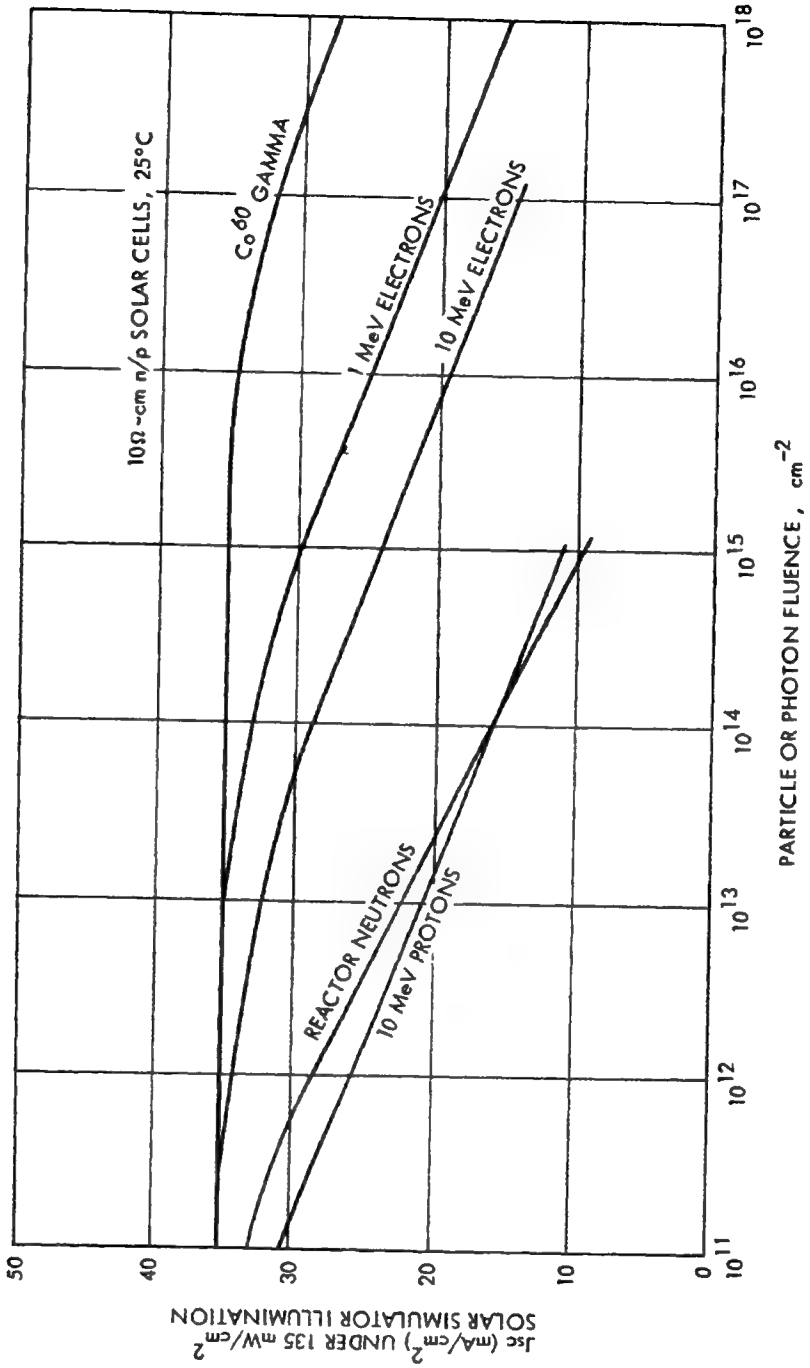

Figure 8-2. Variation of Solar Cell Short Circuit Current Density with Fluence for Various Radiations

The percentages in the tables should be used as rough estimate. Though great effort was made to ensure that the solar simulator was calibrated to AM0, minor fluctuations in the solar simulator or surrounding light, caused noticeable fluctuations in the intensity of the light. Such fluctuations on small cells, like the test cells, would cause a significant change in output. However, these test results are in general agreement and do indicate that the damaged cells were partially annealed.

The results, however, did not achieve the same degree of annealing that was produced in previous current-injection/thermal annealing research [Ref. 2:p. 36], so another test was conducted to explore the difference in results.

This test was conducted using Cell B, and the intent was to duplicate the previous current-injection method described in Reference 2 to see if further annealing would take place. Cell B was placed on a 1 ohm resistor and the temperature was raised to an average of 95°C. An external DC power supply was used to forward bias the cell so that 60 mA of current was injected into the cell. This experiment was conducted for 16 hours, however, no further annealing took place using this method.

IX. CONCLUSIONS

In this research a technique for annealing radiation damaged GaAs solar cells using visible laser was introduced. For a proof of concept, an experiment was conducted where sample GaAs cells were irradiated and the resulting performance degradation was recorded. Several attempts to anneal the damaged cells were carried out using a visible laser and the resulting recovery was recorded.

The results show that a laser can induce some annealing in radiation damaged GaAs solar cells. The preliminary results indicated that laser annealing recovered 10 to 20 percent of the lost capabilities. The results, however, did not compare well with previous work where current annealing experiments achieved over 85% recovery of the initial capabilities following electron irradiation [Ref. 2:p. 26]

Further investigation into the results of this research showed that no further annealing took place using the current-injection/thermal annealing method described by both Cypranowski and Clark [Ref. 2:p .45][Ref. 14:p. 54]. The lack of significant recovery can most likely be explained by two factors that differ from previous research. The first is that this research was conducted using the NPS LINAC that produces electrons with 65 MeV energy level. Previous research by Clark and Cypranowski used the linear accelerator located at the Jet Propulsion Laboratory in Pasadena, CA providing electron irradiation with 1 MeV energy level. Due to the different capabilities of the NPS LINAC, the high energy level of the electron irradiation could have caused greater permanent damage to the crystalline structure of the solar cell material than experienced

in previous research. The high energy electrons are capable of penetrating deep into the cell and causing atomic displacements. Very high energy particles can cause a cascading effect, displacing many more atoms, eventually forming permanent stable defects in the lattice [Ref. 1:pp. 149-165]. The fact that cell B did not further anneal even with current-injection, tends to support the above reasoning.

Secondly, this research used a radiation dose equivalent to 10^{15} electrons/cm^2 with the intent of showing a visible degradation so that power recovery due to laser annealing would be readily discernible. The relatively small solar cells degraded 20 percent. In the previous work, research was carried out a much lower dose, resulting in, at most, a 10 percent degradation of the solar cell output parameters.

Further study should include irradiation of solar cells using 1 MeV electron energy to reduce the possibility of induced permanent damage occurrence, and therefore an improvement in recovery should be expected as well.

Test Cells used in future work should be larger in size. The test cells used in this research were of an area of only 12.6 mm^2, which were initially believed to be ideal so that a lower power laser could be used to perform the research. However, this caused some trouble due to the low output of only 3.5 mA (I_{sc}), which made calibration of the solar simulator difficult. Ideally, a cell of similar size as the standard cell used for calibration should be used.

A more powerful laser would be needed so that the laser beam could be expanded to accommodate larger solar cells and still maintain the same power density. Though the

Argon-ion laser produced good results, experimentation with slightly longer wavelength should be tested due to the possible improvement of cell efficiency.

Although the performance recovery was not as high as was originally anticipated, the proof of concept was verified; lasers can be used to anneal radiation damaged solar cells. Laser technology is rapidly improving, and more powerful lasers are being produced which will make power beaming of spacecraft a reality. Future research with improvements in procedural set-up should establish the potential to perform laser annealing for solar arrays.

APPENDIX A. SPECIFICATIONS FOR THE STANDARD SOLAR CELL

SILICON
K6700A
SOLAR CELLS

SPECTRODATA

TYPICAL ELECTRICAL PARAMETERS*

Jsc = 42.5 Milliamperes/cm²
Jmp = 39.6 Milliamperes/cm²
Vmp = 0.500 Volts
Pmp = 19.8 Milliwatts/cm²
Voc = 0.605 Volts
Ff = 0.77
Efficiency 14.6% Minimum Average
***AMO Sunlight (135.3 mw/cm²), 28°C**

RADIATION DEGRADATION*

PARAMETER	$1x10^{13}$	$1x10^{14}$	$1x10^{15}$	$1x10^{16}$
Isc/Isco	0.97	0.95	0.86	0.75
Imp/Impo	0.96	0.94	0.84	0.72
Vmp/Vmpo	0.94	0.92	0.83	0.74
Voc/Voco	0.94	0.92	0.84	0.76
Pmp/Pmpo	0.90	0.86	0.71	0.53

***Fluence e/cm² 1 MeV Electrons**

THERMAL PROPERTIES

Solar Absorptance = 0.79 (CMX)
Solar Absorptance = 0.77 (Fused Silica)
Emittance (Normal) = 0.85 (CMX)
Emittance (Normal) = 0.81 (Fused Silica)

WEIGHT

55 Milligrams/cm² (Bare)

TEMPERATURE COEFFICIENTS

Isc = +22.0 Microamperes/cm²
Vmp = −2.15 Millivolts/°C
Voc = −1.98 Millivolts/°C

APPLICATION NOTES

TYPICAL I-V CHARACTERISTIC CURVE*

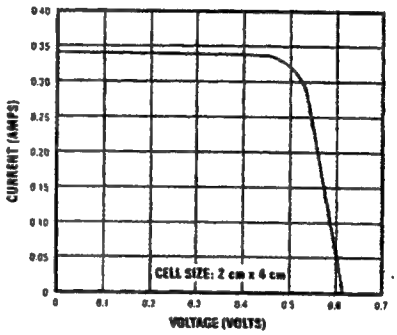

***AMO Sunlight (135.3 mw/cm²), 28°C**

SPECTRAL RESPONSE

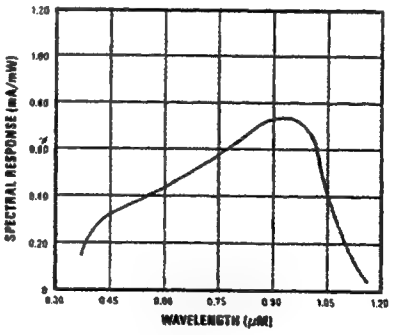

SPECTROLAB, INC.
Subsidiary of Hughes Aircraft Company
12500 Gladstone Avenue
Sylmar, California 91342-5373
TELEPHONE: (818) 365-4811
TWX: 910-496-1750
TELECOPIER: (818) 361-5102
TLX: 182881 SPECTLLM SYLM

SPECTRODATA

SILICON
K6700A
SOLAR CELLS

FEATURES

- **HIGH CONVERSION EFFICIENCY**
  - Beginning of Life
  - End of Life
- **HIGH STATE-OF-THE-ART RELIABILITY**
- **OPTIMIZED OPERATING TEMPERATURE**
- **HARDENED APPLICATIONS**
  - Space Environmental Effects:
    - Military
    - Commercial
  - Terrestrial Power
  - Consumer Products
- **LOW COST**
  - Standard Products
  - Custom Products

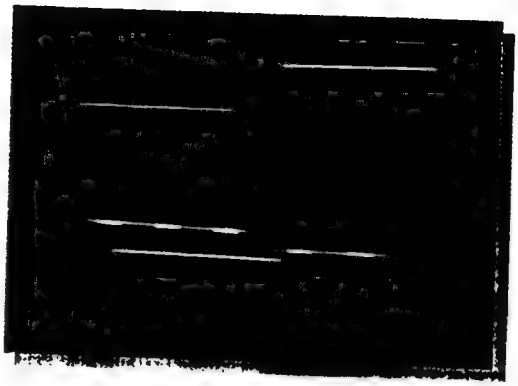

PRODUCT DESCRIPTION

Standard/Special Product	Standard
Resistivity (p-type)	10 Ohm-cm
Crystal Orientation	1 - 0 - 0
Method of Growth	Czochralski
Shallow Junction	0.15 Micron
Metallization (Front)	TiPdAg
Metallization (Back)	AlTiPdAg
Anti-Reflective Coating	Multi-Layer
Back Surface Reflector	Aluminum
Back Surface Field	Aluminum
Sculptured Front Surface	No
Thickness	200 Microns
Sizes	Up to 8x8 cm
Weldable	Yes
Solderable	Sn62 Solder (QQ-S-571)

NOTE: Other variations are available upon request.

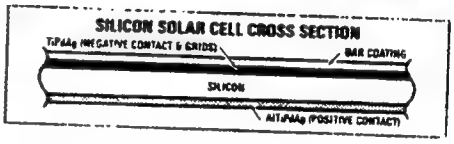

TYPICAL QUALIFICATION TEST RESULTS *(Nominal Degradation)*

TEST	DESCRIPTION	RESULTS
Humidity	+45°C, 90% RH Min., 30 Days	<1.5%
Thermal Cycle	+80°C to -180°C, 3000 Cycles	<2.5%
Thermal Shock	+140°C to -185°C, 5 Cycles	<1.5%
Thermal Soak	+140°C for 168 Hrs., $5x10^{-5}$ torr	<1.5%
Radiation	Characterized thru $1x10^{16}$ 1 MeV e/cm²	—
Pull Test	90° Pull, Standard Tab	>250 gms

SPECTROLAB, INC.
Subsidiary of Hughes Aircraft Company
12500 Gladstone Avenue
Sylmar, California 91342-5373
TELEPHONE: (818) 365-4611
TWX: 910-496-1750
TELECOPIER: (818) 361-5102
TLX: 182881 SPECTILLM SYLM

APPENDIX B. SPECIFICATIONS FOR THE HP 6626A PROGRAMMABLE POWER SUPPLY

PERFORMANCE SPECIFICATIONS: (0 to 55 °C unless otherwise specified)

Output Ranges: All outputs will accept voltage programming commands 1% higher than those listed and current programming commands 3% higher than those listed.

Output Power	**25 Watt Output**		**50 Watt Output**	
Output Range	Lo Range	Hi Range	Lo Range	Hi Range
Output Volts	0-7 V	0-50 V	0-16 V	0-50 V
Output Amps	0-15 mA	0-500 mA	0-200 mA	0-2 A
Load Effect (Regulation):				
Voltage	0.5 mV	0.5 mV	0.5 mV	0.5 mV
+Current	0.005 mA	0.005 mA	0.01 mA	0.01 mA
Source Effect:				
Voltage	0.5 mV	0.5 mV	0.5 mV	0.5 mV
+Current	0.005 mA	0.005 mA	0.01 mA	0.01 mA
Load Cross Regulation:				
Voltage	0.25 mV	0.25 mV	0.25 mV	0.25 mV
+Current	0.005 mA	0.005 mA	0.01 mA	0.01 mA
Programming Accuracy:				
Voltage	0.016% + 1.5 mV	0.016% + 10 mV	0.016% + 3 mV	0.016 + 10 mV
+Current	0.04% + 15 μA	0.04% + 100 μA	0.04% + 185 μA	0.04% + 500 μA
OVP	0.13% + 475 mV	0.13% + 475 mV	0.13% + 475 mV	0.13% + 475 mV
Measurement/ Readback Accuracy*				
Voltage	0.016% + 2 mV	0.016% + 10 mV	0.016% + 3.5 mV	0.016% + 10 mV
± Current	0.03% + 15 μA	0.03% + 130 μA	0.04% + 250 μA	0.04% + 550 μA

Load Transient Recovery Time :(all outputs)

75 μS maximum to recover to within 75 mV of nominal value following a load change from 0.1 A to 100% of the maximum rated current

* For a ±5 ° C range about the calibration temperature

Output Power	**25 Watt Output**		**50 Watt Output**	
Output Range	Lo Range	Hi Range	Lo Range	Hi Range
Output Volts	0-7 V	0-50 V	0-16 V	0-50 V
Output Amps	0-15 mA	0-500 mA	0-200 mA	0-2 A
Temperature Coefficient-Programming:				
Voltage	(0.003% + 0.1 mV) per° C	(0.003% + 0.1 mV) per° C	(0.003% + 0.1 mV) per° C	(0.003% + 0.1 mV) per° C
+ Current	(0.0035% + 1.5 μA) per° C	(0.0035% + 6 μA) per° C	(0.0035% + 30 μA) per° C	(0.0035% + 50 μA) per° C
OVP	(0.013% + 1 mV) per° C	(0.013% + 2 mV) per° C	(0.013% + 1 mV) per° C	(0.013% + 2 mV) per° C
Temperature Coefficient-Measurement:				
Voltage	(0.002% + 0.1 mV) per° C + 0.5 mV	(0.002% + 0.1 mV) per° C + 4 mV	(0.002% + 0.1 mV) per° C + 1 mV	(0.002% + 0.1 mV per° C + 4 mV
± Current	(0.0025% + 1.5 μA) per° C + 1 μA	(0.0025% + 10 μA) per° C + 40 μA	(0.0025% + 20 μA) per° C + 15 μA	(0.0025% + 50 μA) per° C + 150μA
Long Term Drift: (In an 8 hour period following a 30 minute warm up)				
Voltage	0.006% + 0.5 mV	0.006% + 2 mV	0.006% + 0.5 mV	0.006% + 2 mV
+ Current	0.01% + 5 μA	0.01% + 20 μA	0.01% + 40 μA	0.01% + 60 μA
Short Term Drift: (Within 30 minutes after a line and/or load change):				
Voltage	0.002 + 0.5 mV	0.002 + 1 mV	0.002 + 0.5 mV	0.002 + 1 mV
+ Current	0.01% + 2 μA	0.01% + 20 μA	0.01% + 25 μA	0.01% + 60 μA
Maximum Output Noise: (PARD) (20 Hz—20 MHz)				
CV pk-to-pk	3 mV	3 mV	3 mV	3 mV
CV rms	0.5 mV	0.5 mV	0.5 mV	0.5 mV
+ CC rms	0.1 mA	0.1 mA	0.1 mA	0.1 mA

Isolation:

No output terminal may be more that 240 Vdc from any other terminal or from chassis ground. Also, no overvoltage terminal may be more than 240 Vdc from any other terminal or chassis ground.

Remote Sense Capability:

Outputs can maintain specifications with up to 10 volt total in the remote sense leads.

Input Line Requirements:

Note at low line, the supply will operate with up to ¾ ohm line resistance

Amplitude	+6% to −13% of nominal line voltage
Frequency	47 to 66 Hz
Maximum Power	550 Watts

PERFORMANCE SPECIFICATIONS: (0 to 55 °C unless otherwise specified)

High Line Inrush Current:	100 V Opt	120 V Opt	220 V Opt	240 V Opt
Peak Value:	85 A	85 A	50 A	50 A
rms Value:	6.3 A	5.7 A	3.0 A	3.0A
Fuse Rating:	8 A	8 A	4 A	4 A

HP-IB Interface Capabilities:

SH1, AH1, T6, L4, SR1, RL1, PP1, DC1, DT0, C0, E1

SUPPLEMENTAL CHARACTERISTICS

Output Power	**25 Watt Output**		**50 Watt Output**	
Output Range	Lo Range	Hi Range	Lo Range	Hi Range
Output Volts	0-7 V	0-50 V	0-16 V	0-50 V
Output Amps	0-15 mA	0-500 mA	0-200 mA	0-2 A
Programming Resolution:				
Voltage	460 μV	3.2 mV	1 mV	3.2 mV
+ Current	1 μA	33 μA	13 μA	131 μA
OVP	230 mV	230 mV	230 mV	230 mV
Readback Resolution:				
Voltage	483 μV	3.3 mV	1.1 mV	3.3 mV
+ Current	1 μA	48 μA	14 μA	160 μA
− Current	1 μA	37 μA	14 μA	151 μA
Fixed Overvoltage Protection: (Measured at output terminals +V and −V)				
Minimum	56 V	56 V	56 V	56 V
Nominal	60 V	60 V	60 V	60 V
Maximum	64 V	64 V	64 V	64 V

Current Sink Capability:

25 Watt output: 0.50 A
50 Watt output: 1.0 A (2.0 A below 16 V)

Command Processing Time: (see Figure 1-3)
7 milliseconds typical (with front panel disabled). Using STD and RCL commands allows you to change all the voltage and current settings in about 10 mS with front panel disabled).

Maximum Output Programming:				
Response Time	6 mS	6 mS	6 mS	6 mS
Settling Band	50 mV	50 mV	50 mV	50 mV
Maximum Time				
Constant	750 μS	750 μ S	750 μS	750 μS

Series and Parallel operation:

Two outputs can be operated directly in parallel or can be connected for straight series operation. Refer to Section IV for more information.

APPENDIX C. SOLAR CELL I-V PLOTTING PROGRAM

```
80  CLEAR SCREEN
90  DUMP DEVICE IS 701
100 PRINT "INPUT LOW VOLTAGE RANGE 0.00"
110 ENTER KBD; L_volt
120 PRINT "INPUT HIGH VOLTAGE RANGE 00.00"
130 ENTER KBD; H_volt
140 PRINT "INPUT MAX CURRENT RANGE, 4-(50mA) 2-(100mA) 1-(1A)
    40-(5mA)."
150 ENTER  KBD;I_RANGE
151 IF I_RANGE=4 THEN 160
152 IF I_RANGE=2 THEN 160
153 IF I_RANGE=1 THEN 155
154 IF I_RANGE=40 THEN 160
155 C_RANGE=I_RANGE*100
156 GOTO 170
160 C_RANGE=I_RANGE*500
170 CLEAR SCREEN
180 V_STEP=.01
190 X_axis=H_volt-L_volt
200 X_step=120/(X_AXIS/V_STEP)
210 X_label=L_volt
220 V_RANGE=I_RANGE
230 IF I_RANGE=1 THEN 250
240 V_RANGE=V_RANGE*5
250 V_RANGE=V_RANGE*1
260 ASSIGN @Ps TO 705
```

```
270 OUTPUT @Ps; "OUT 4,0"
280 VIEWPORT 20,120,20,90
290 AXES 5,5,0,0,2,2,3
300 FRAME
310 CLIP OFF
320 CSIZE 3
330 MOVE 10,100
340 LORG 1
350 LABEL "I-V CHARACTERISTICS OF A GaAs SOLAR CELL;
    DATES$(TIMEDATE)
360 MOVE 55,-10
370 LORG 3
380 LABEL "VOLTAGE - V"
390 MOVE -15,30
400 DEG
410 LDIR 90
420 LORG 3
430 LABEL "CURRENT - I(AMPS)"
440 LDIR 0
450 LORG 2
460 MOVE -10,20
470 LABEL USING ".DDD";.2/V_RANGE
480 MOVE -10,40
490 LABEL USING ".DDD";.4/V_RANGE
500 MOVE -10,60
510 LABEL USING ".DDD";.6/V_RANGE
520 MOVE -10,80
530 LABEL USING ".DDD";.8/V_RANGE
540 MOVE -10,100
550 LABEL USING "D.DD";1.0/V_RANGE
```

```
560 LORG 6
570 MOVE 0,-5
580 LABEL X_label
590 LET Y=-5
600 FOR X=20 TO 120 STEP 20
610 LET X_label=X_label+(20/X_step*V_step)
620 MOVE X,Y
630 LABEL USING "DD.DDD";X_label
640 NEXT X
650 !START MEASUREMENTS HERE
660 CLIP ON
670 OUTPUT @Ps;"OUT 4,1"
680 LET V=L_volt
690 FOR X=0 TO 120 STEP X_step
700 OUTPUT @Ps;"VSET 4";V
710 OUTPUT @Ps;"IOUT? 4"
720 ENTER @Ps;C
730 IF C>0 THEN 800
740 I=ABS(C)
750 Y=I*C_RANGE]
751 OUTPUT 26;C;","; v;CHR$(13);CHR$(10);
760 MOVE (X-(X_step/4)),Y
770 DRAW X,Y
780 V=V+V_step
790 NEXT X
800 OUPUT @Ps;"OUT 4,0"
810 END
```

APPENDIX D. GALIUM ARSENIDE SOLAR CELL DATA PLOTS

Current-Voltage curves and Power-Voltage curves were plotted following both the irradiation and annealing stages of this research. These graphs show before radiation, after radiation, and after annealing curves. In addition, the legend on each plot indicates I_{sc} or P_{max} at each of the three stages.

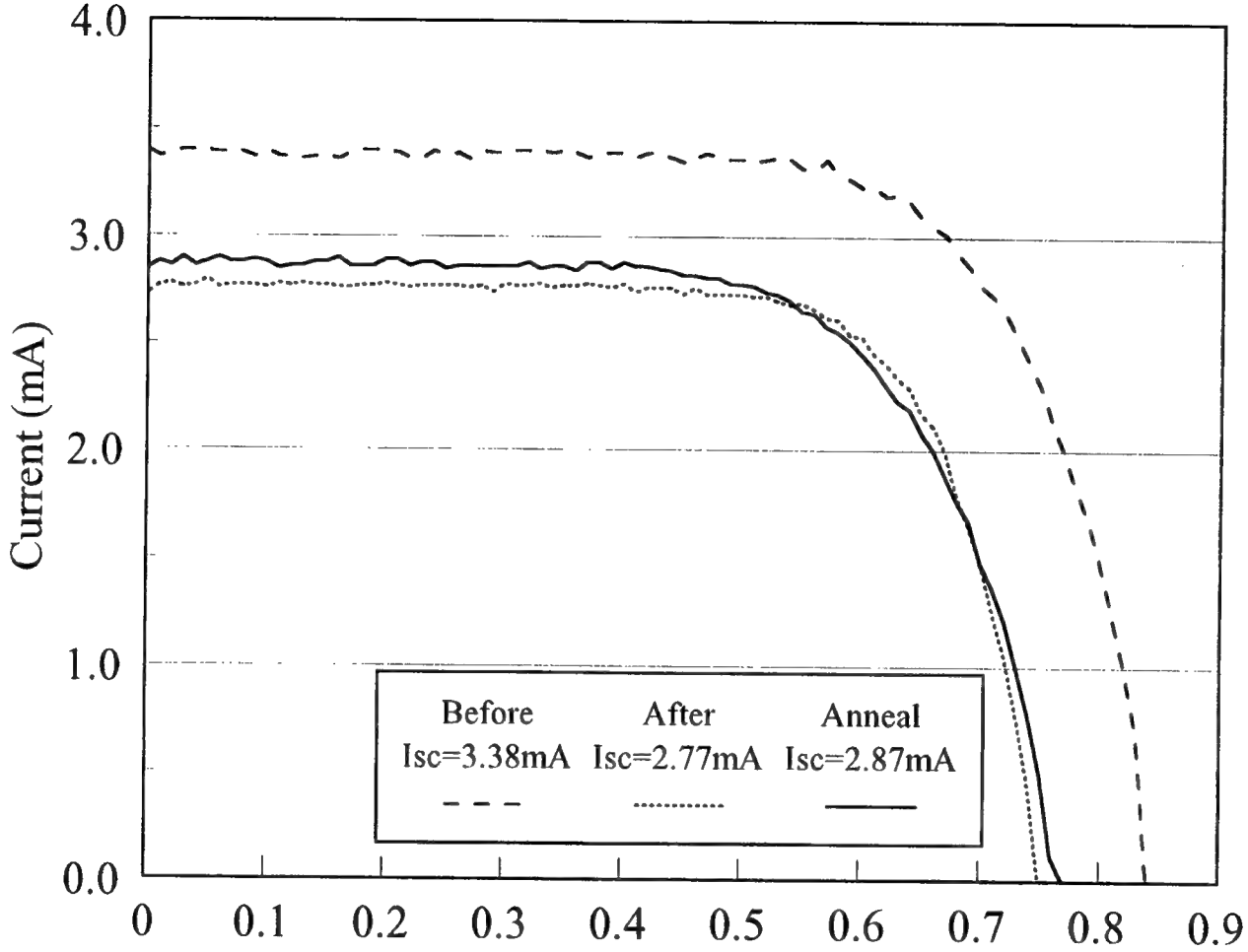

I-V Curves for Cell A Before Radiation, After Radiation, and Annealed

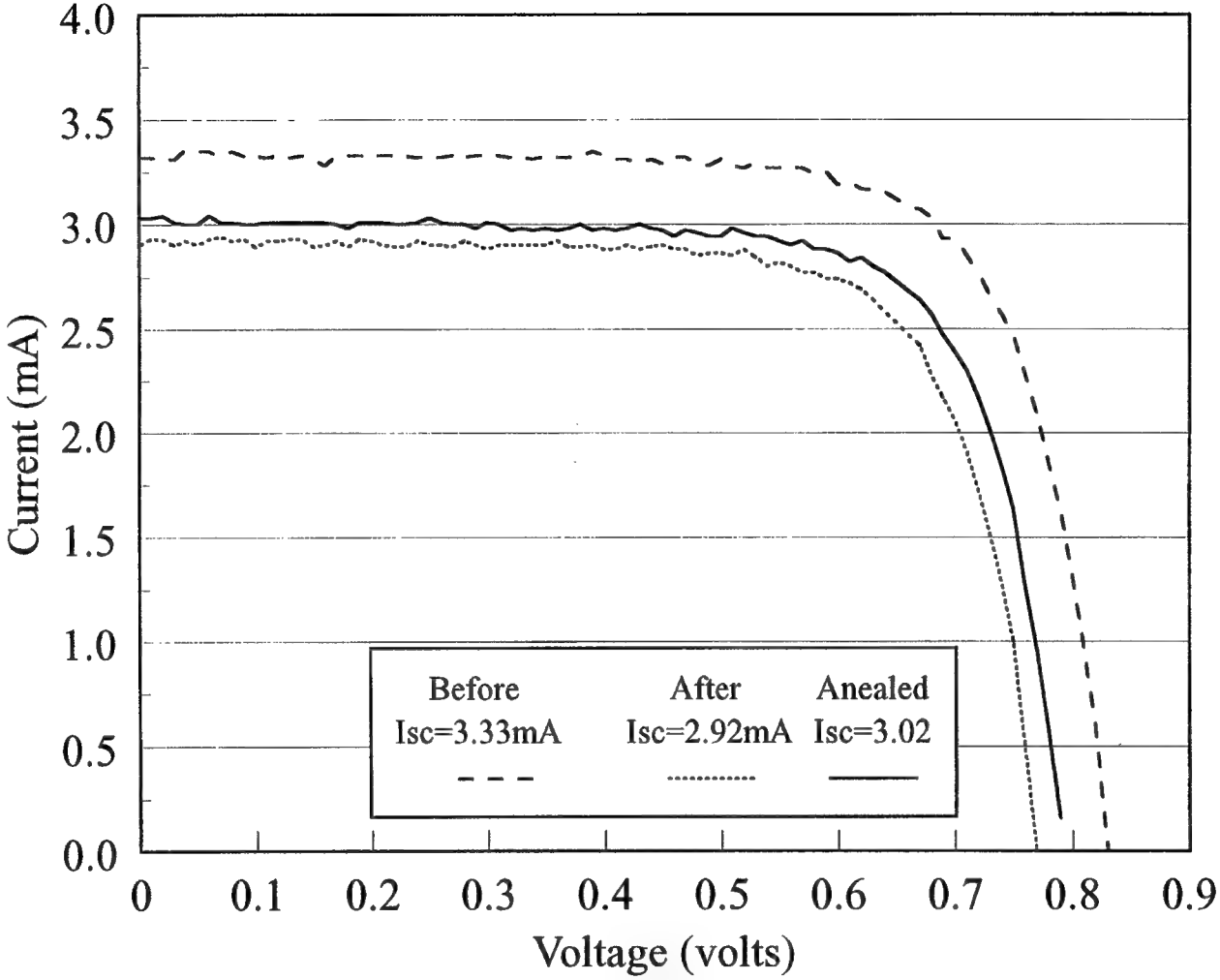

I-V Curves for Cell B Before Radiation, After Radiation, and Annealed

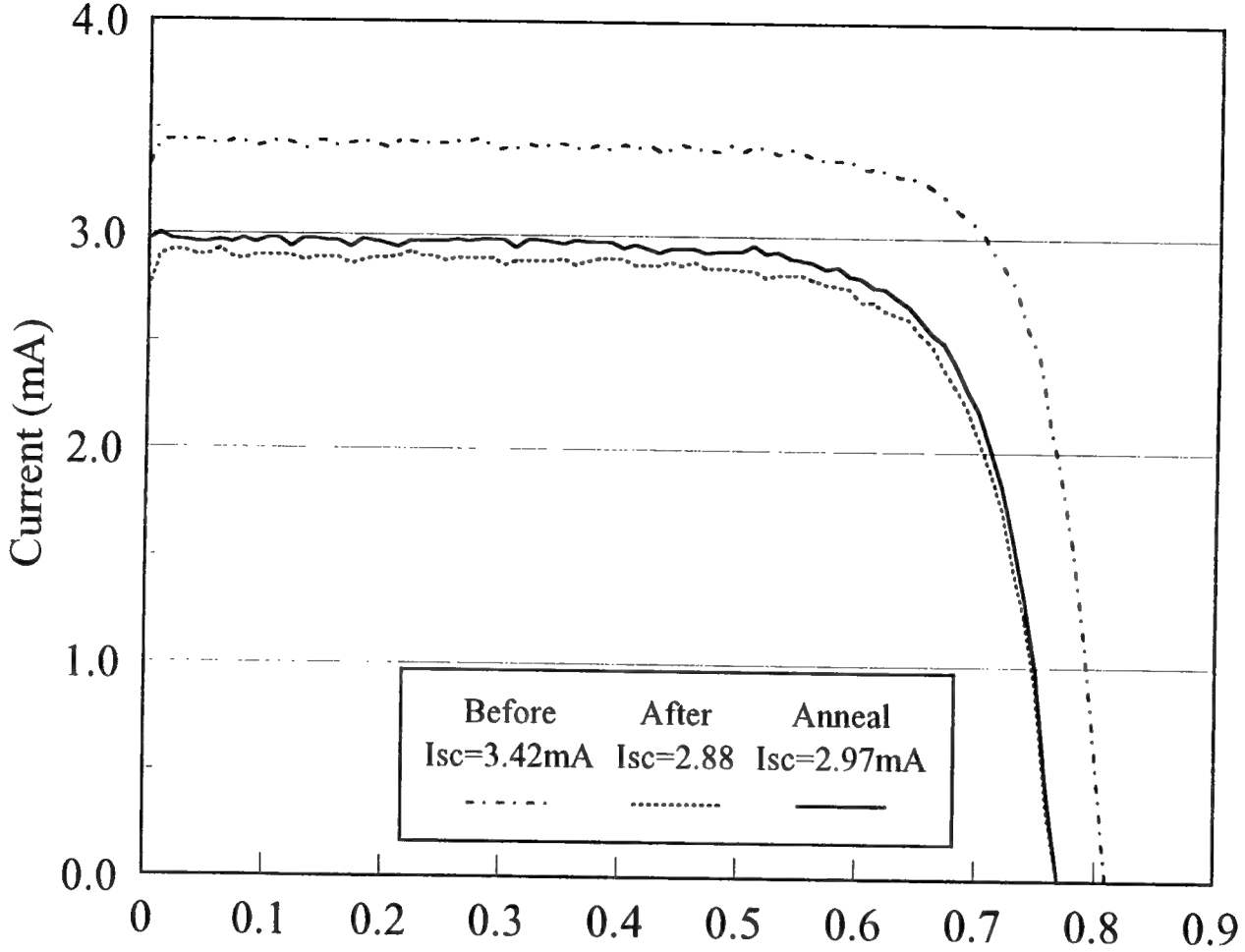

I-V Curves for Cell D Before Radiation, After Radiation, and Annealed

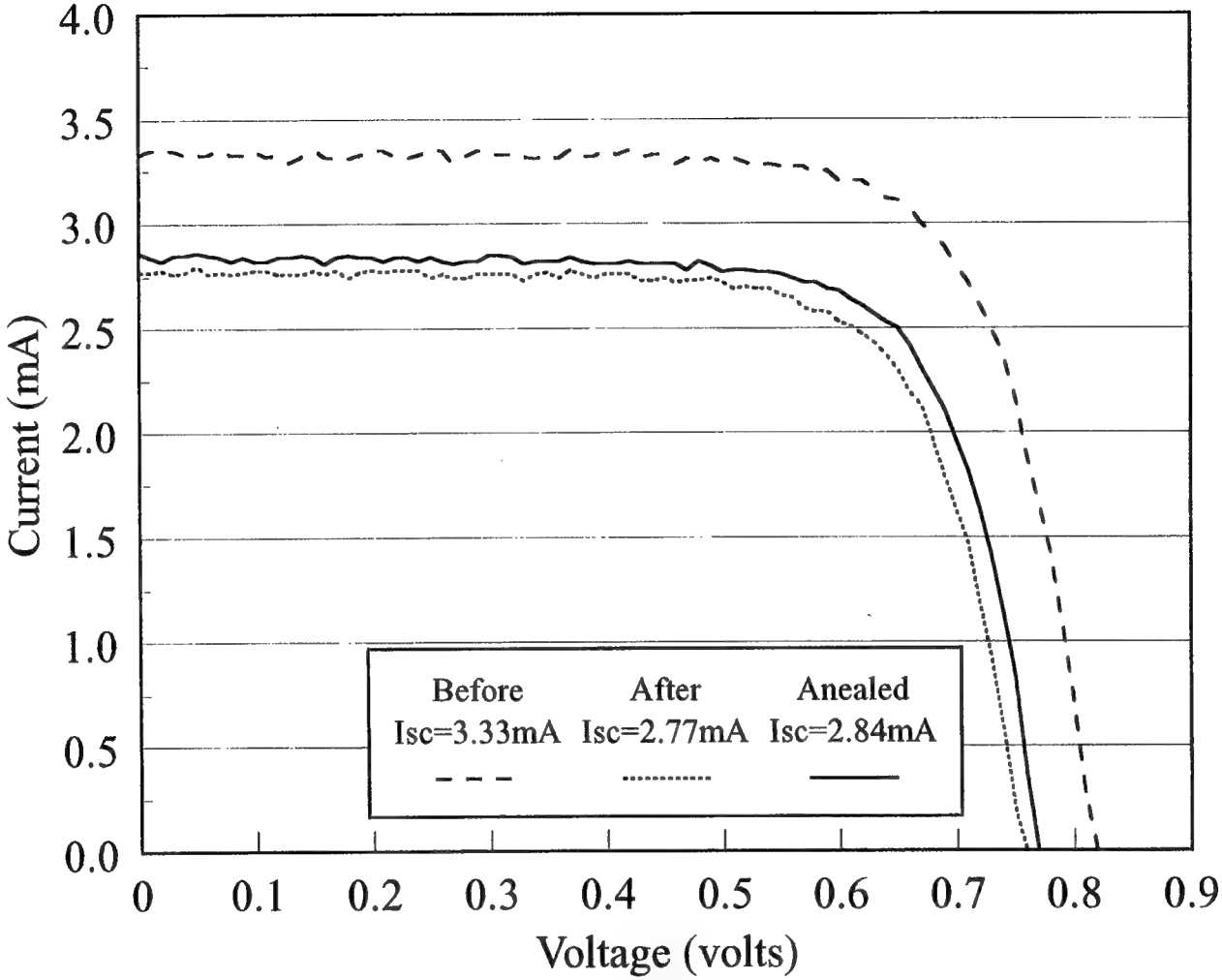

I-V Curves for Cell E Before Radiation, After Radiation, and Annealed

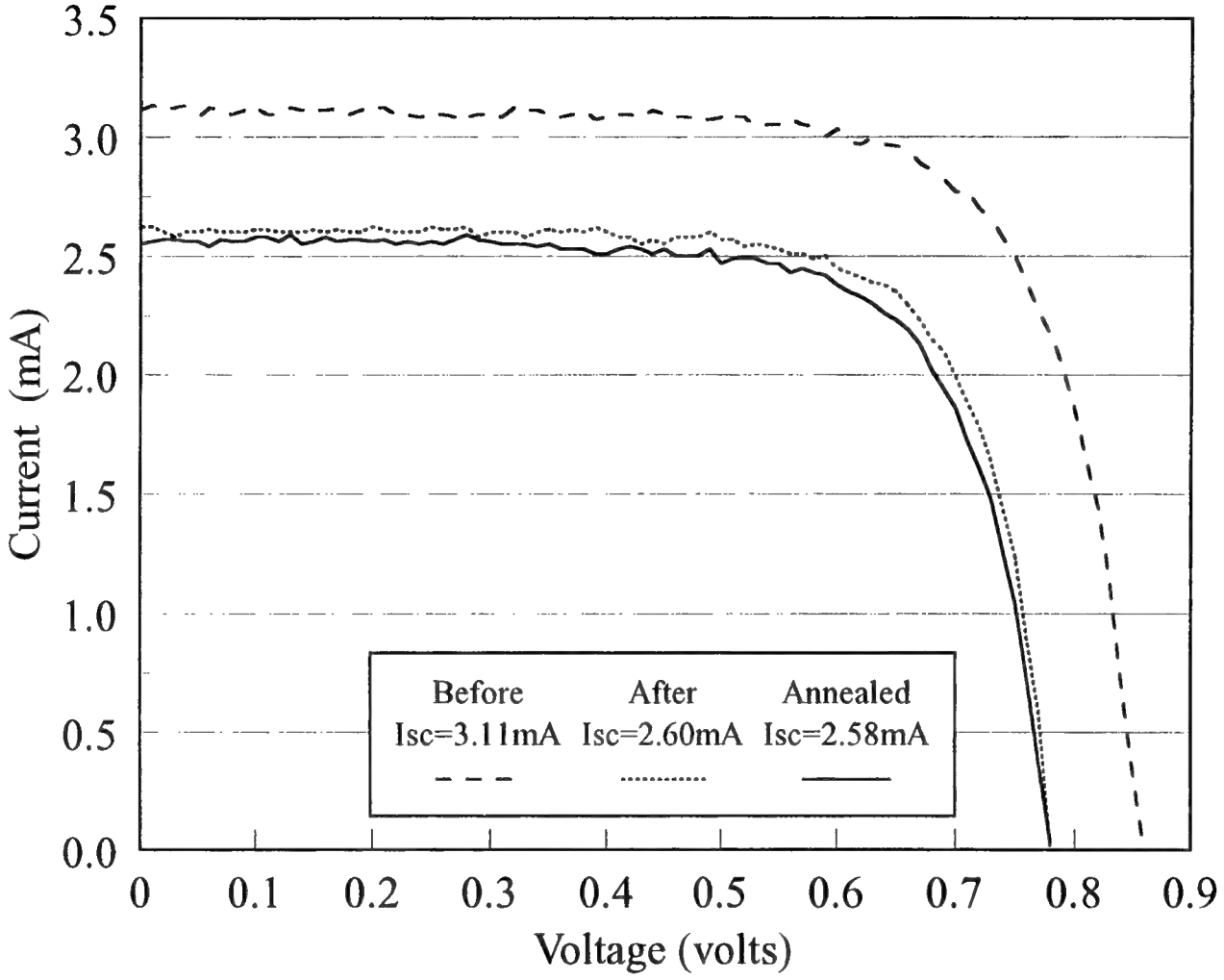

I-V Curves for Cell F Before Radiation, After Radiation, and Annealed

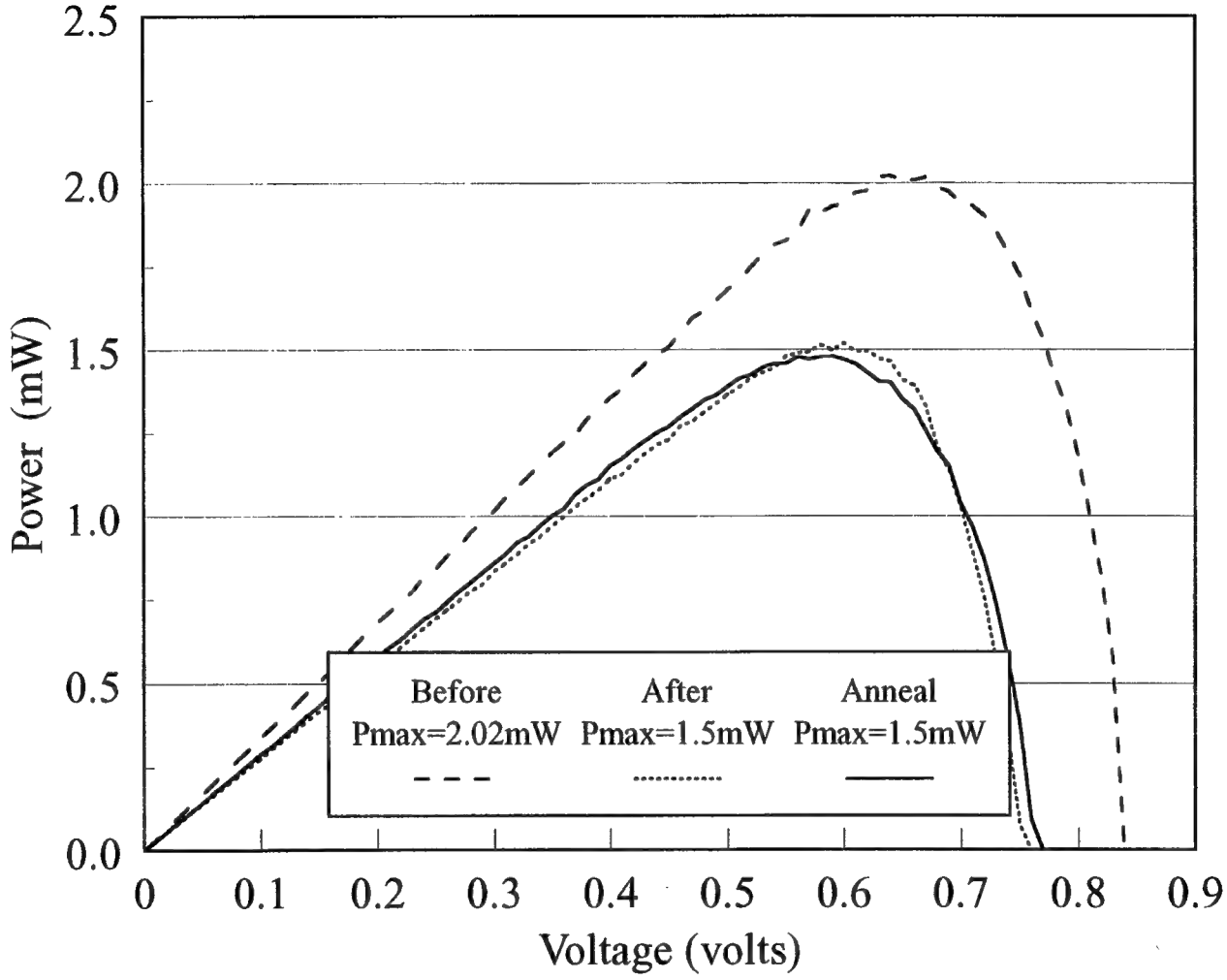

P-V Curves for Cell A Before Radiation, After Radiation, and Annealed

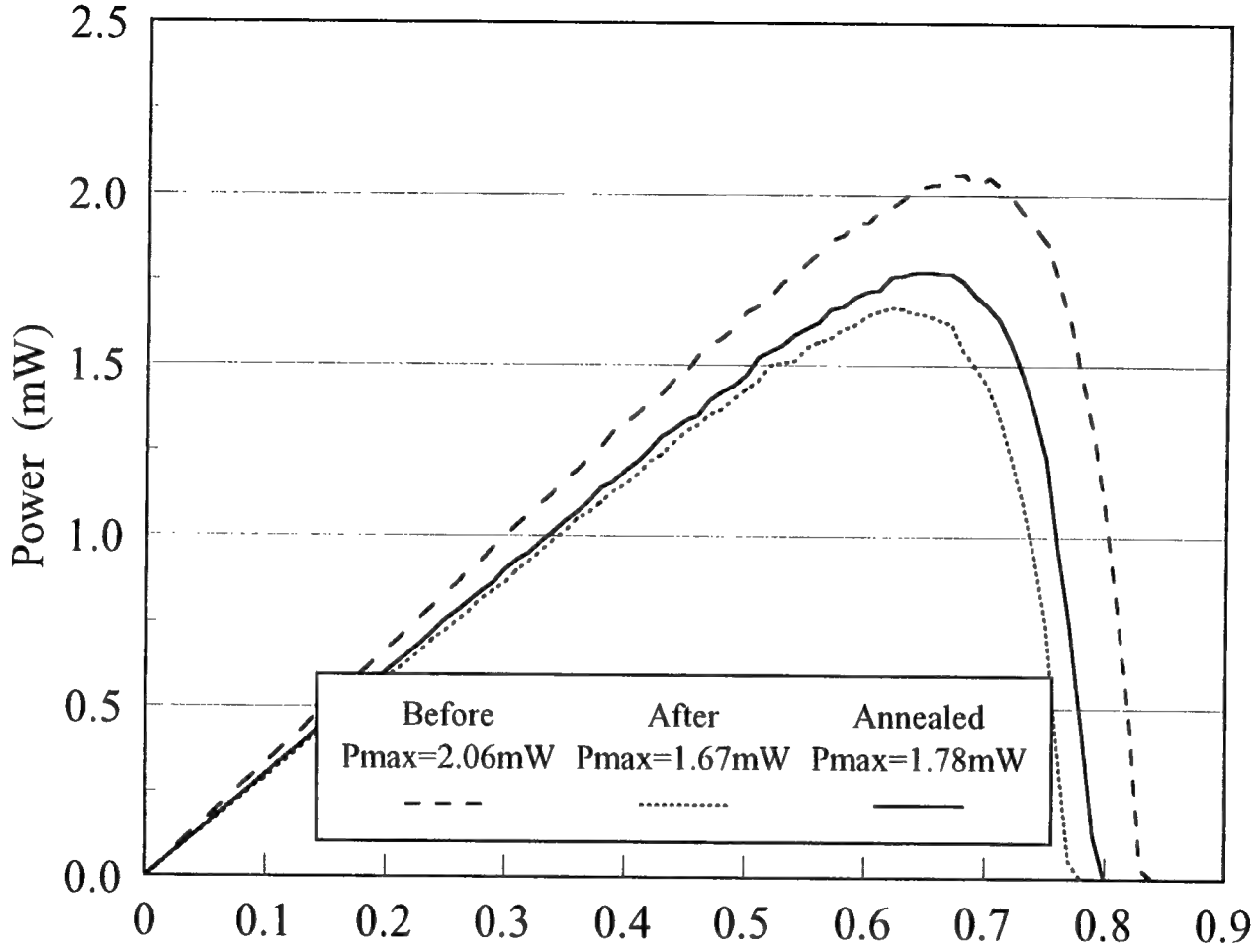

P-V Curves for Cell B Before Radiation, After Radiation, and Annealed

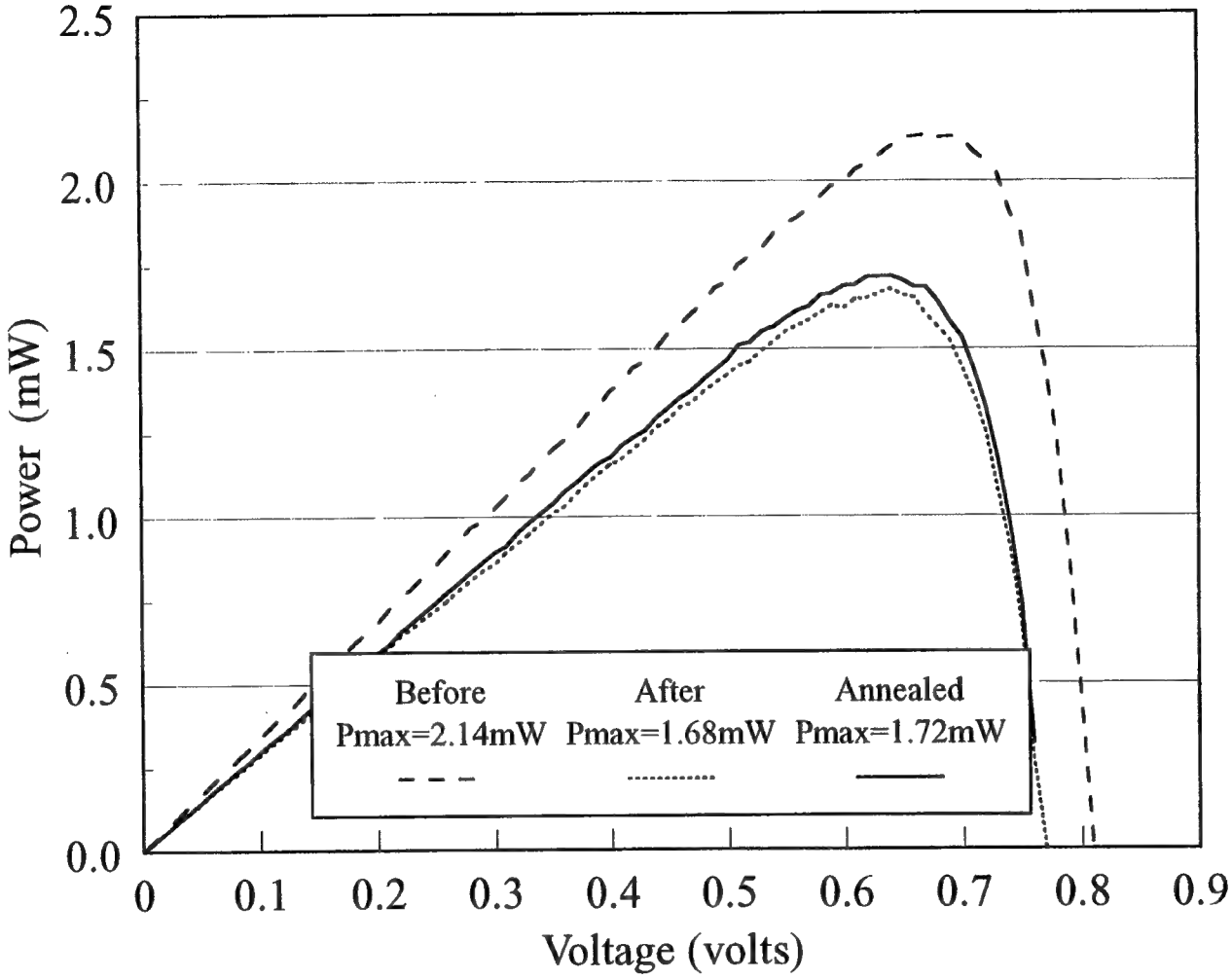

P-V Curves for Cell D Before Radiation, After Radiation, and Annealed

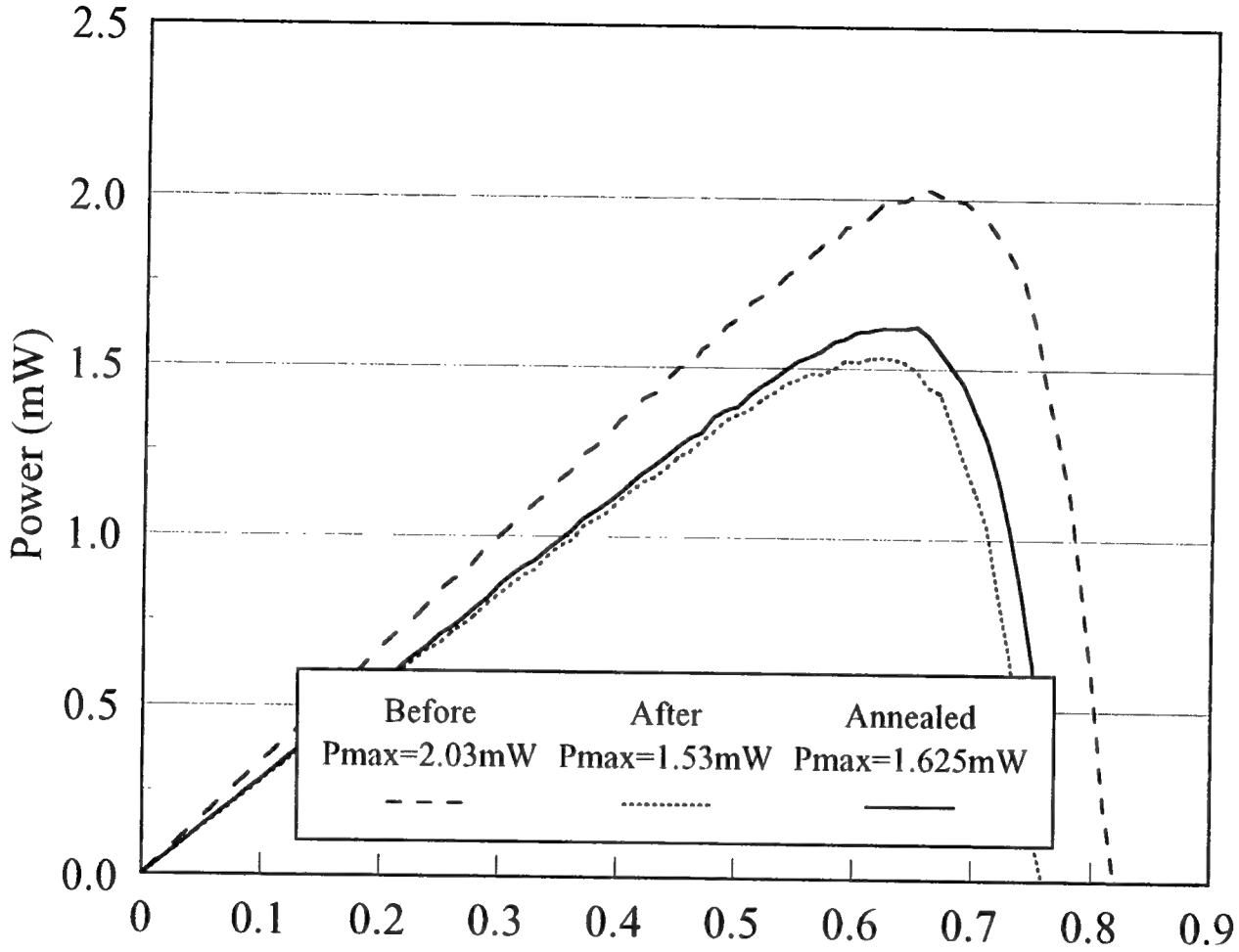

P-V Curves for Cell E Before Radiation, After Radiation, and Annealed

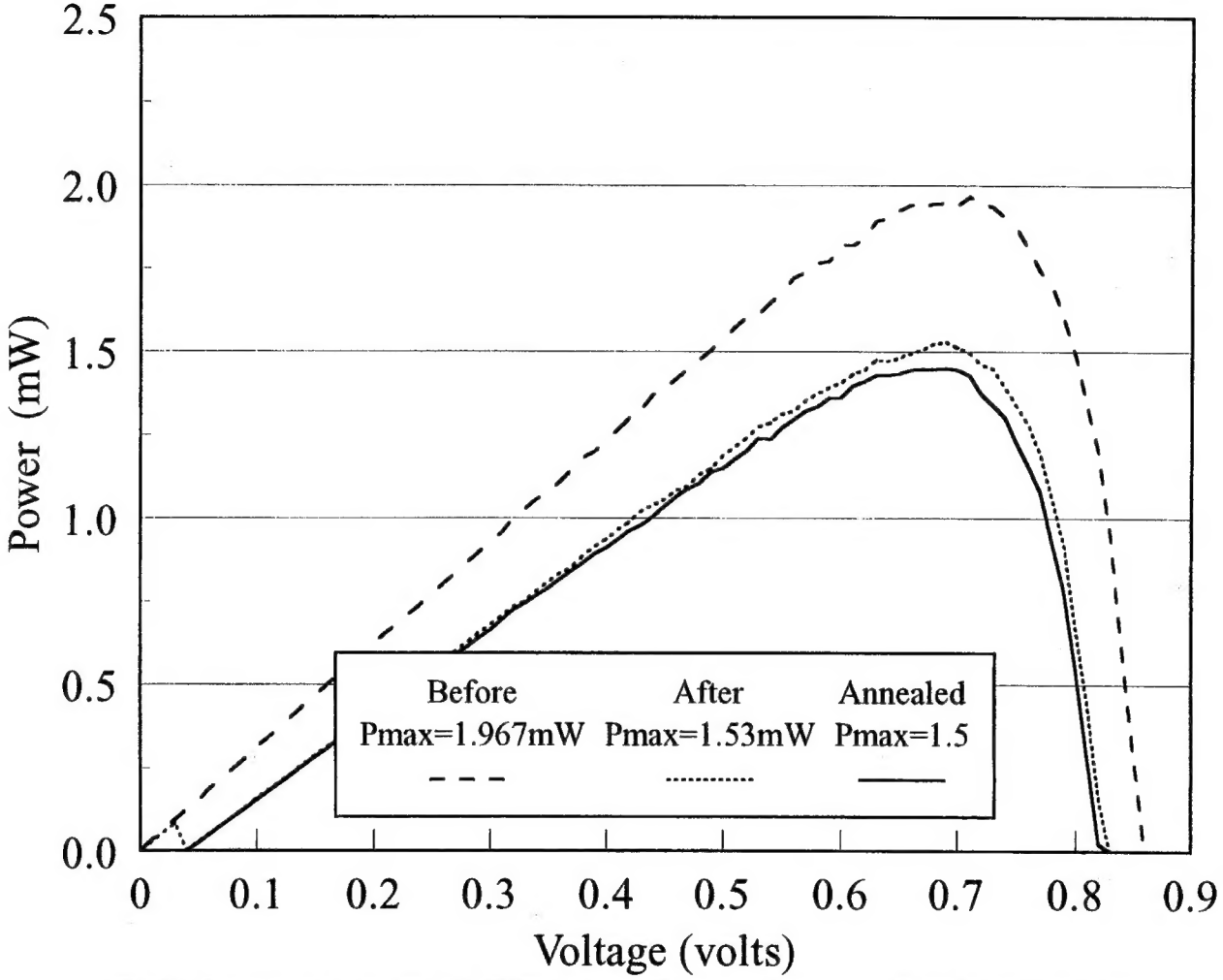

P-V Curves for Cell F Before Radiation, After Radiation, and Annealed

LIST OF REFERENCES

1. Hovel, H.J., Semiconductors and Semimetals, Volume 11, Solar Cells, Academic Press, New York, New York, 1975.

2. Cypranowski, C., Power Recovery of Radiation-Damaged Gallium Arsenide and Indium Phoshide Solar Cells, Master's Thesis, Naval Postgraduate School, Monterey, California, December 1989.

3. Landis, G.A., Photovoltaic Receivers for Laser Beamed Power in Space, Twenty Second IEEE Photovoltaic Specialists Conference, pp. 1494-1502, 1991.

4. Feltry, J.R., "DOE Reactor-Pumped Laser Program," paper presented at NPS Space Systems Seminar, Monterey, California, June 1994.

5. Pivirotto, T.J., Annealing Radiation Damaged Silicon Solar Cells with a Copper Halide Laser, Space Photovoltaic Research and Technology, pp. 277-280, 1980.

6. Hu, C., and White, R.M., Solar Cells, McGraw-Hill Book Co., New York, New York, 1983.

7. Pinzon, D., Analysis of Radiation Damaged and Annealed Gallium Arsenide and Indium Phosphide Solar Cells Using Deep Level Transient Spectroscopy Techniques, Master's Thesis, Naval Postgraduate School, Monterey, California, March 1991.

8. Elachi, C., Introduction to the Physics and Techniques of Remote Sensing, John Wiley & Sons Inc., New York, New York, p. 47, 1987.

9. Greco, G., and Misiano, C., Electron and Proton Damage on Silicon Solar Cells, Proceedings of the International Colloquium, pp. 639-650, 1970.

10. Rivet, S., and Clark, J., "Radiation Effects on Integrated Circuits," The Space Radiation Environment, Harris Semiconductor, Melbourne, Florida, September 1993.

11. Rauschenbach, H.S., Solar Cell Array Design Handbook, Van Nostrand Reinhold Co., New York, New York, 1980.

12. Jet Propulsion Laboratory Publication 82-69, Solar Cell Radiation Handbook, Third Edition, November 1982.

13. Larin, F., Radiation Effects in Semiconductor Devices, John Wiley & Sons Inc., New York, New York, 1968.

14. Clark, T.F., An Experimental Test of Minority Carrier Annealing on Gallium Arsenide Solar Cells Using Forward-Biased Current, Master's Thesis, Naval Postgraduate School, Monterey, California, September 1986.

15. Loo, R.Y., Knechtli, R.C., and Kamath, G.S., Periodic Annealing of Radiation Damage in GaAs Solar Cells, Space Photovoltaic Research and Technology, pp. 249-250, 1980.

16. Michael, S., Cypranowski, C., and Anspaugh, B., Forward-Biased Current Annealing of Radiation Degraded Indium Phosphide and Gallium Arsenide Solar Cells, Twenty First IEEE Photovoltaic Specialists Conference, pp.1178-1183, 1990.

17. Stievenard, D., and Bourgoin, J.C., Degradation and Recovery of GaAs Solar Cells Under Electron Irradiation, Seventeenth IEEE Photovoltaic Specialists Conference, pp. 1103-1107, 1984.

18. Halliday, D., and Resnick, R., Fundamentals of Physics, John Wiley & Sons Inc., New York, New York, pp. 1039-1048, 1988.

19. Yariv, A., Optical Electronics, Saunders College Publishing, Chicago, Illinois, pp. 244-245, 1991.

20. Kirkpatrick, A.R., Neal, W.R., and Minnucci, J.A., "Annealing of Radiation Damage in Silicon Solar Cells", Phase I Report, Simulation Physics, March 1977.

21. Minnucci. J.A., Matthei, K.W., and Kirkpatrick, A.R., In-Situ Annealing of Space Radiation Damage, Thirteenth IEEE Photovoltaic Specialists Conference, pp. 586-589, June 1978.

22. Barnet, M.T., and Cunneen, W.J., Design and Performance of the Electron Linear Accelerator at the U.S. Nav96al Postgraduate School, Master's Thesis, Naval Postgraduate School, Monterey, California, May 1966.

23. Foley, J.K., 30 MeV Electron Beam Irradiation Effects on GaAs LEDs, Master's Thesis, Naval Postgraduate School, Monterey, California, June 1985.

INITIAL DISTRIBUTION LIST

1.	Defense Technical Information Center Cameron Station Alexandria, VA 22304-6145	2
2.	Library, Code 52 Naval Postgraduate School Monterey, CA 93943-5101	2
3.	Chairman, Code EC Department of Electrical and Computer Engineering Naval Postgraduate School Monterey, CA 93943-5121	1
4.	Professor S. Michael, Code EC/Mi Department of Electrical and Computer Engineering Naval Postgraduate School Monterey, CA 93943-5121	4
5.	Professor R. Ashton, Code EC/As Department of Electrical and Computer Engineering Naval Postgraduate School Monterey, CA 93943-5121	1
6.	LCDR Richard D. Kramer 455 Grande Vista Milford, MI 48380	2